UNIVERSITY OF AMSTERDAM

UvA-DARE (Digital Academic Repository)

2vββ spectrum in chiral effective field theory

el Morabit, Saad; Bouabid, Ryan; Cirigliano, Vincenzo; de Vries, Jordy; Gráf, Lukáš; Mereghetti, Emanuele

DOI
10.48550/arXiv.2412.14160
10.1007/JHEP06(2025)082

Publication date
2025

Document Version
Final published version

Published in
Journal of High Energy Physics

License
CC BY

Link to publication

Citation for published version (APA):
el Morabit, S., Bouabid, R., Cirigliano, V., de Vries, J., Gráf, L., & Mereghetti, E. (2025). 2vββ spectrum in chiral effective field theory. *Journal of High Energy Physics*, *2025*(6), Article 82. https://doi.org/10.48550/arXiv.2412.14160, https://doi.org/10.1007/JHEP06(2025)082

General rights
It is not permitted to download or to forward/distribute the text or part of it without the consent of the author(s) and/or copyright holder(s), other than for strictly personal, individual use, unless the work is under an open content license (like Creative Commons).

Disclaimer/Complaints regulations
If you believe that digital publication of certain material infringes any of your rights or (privacy) interests, please let the Library know, stating your reasons. In case of a legitimate complaint, the Library will make the material inaccessible and/or remove it from the website. Please Ask the Library: https://uba.uva.nl/en/contact, or a letter to: Library of the University of Amsterdam, Secretariat, P.O. Box 19185, 1000 GD Amsterdam, The Netherlands. You will be contacted as soon as possible.
UvA-DARE is a service provided by the library of the University of Amsterdam (https://dare.uva.nl)

Download date:18 Nov 2026

Published for SISSA by Springer

Received: January 27, 2025
Accepted: April 10, 2025
Published: June 11, 2025

$2\nu\beta\beta$ spectrum in chiral effective field theory

Saad el Morabit,[a,b] **Ryan Bouabid**,[c] **Vincenzo Cirigliano**,[d] **Jordy de Vries**,[a,b] **Lukáš Gráf**[b,e] **and Emanuele Mereghetti**[f]

[a] *Institute for Theoretical Physics Amsterdam, University of Amsterdam, Science Park 904, 1098 XH Amsterdam, The Netherlands*
[b] *Nikhef, Theory Group, Science Park 105, 1098 XG, Amsterdam, The Netherlands*
[c] *Department of Physics, Duke University, Durham, NC, 27708, U.S.A.*
[d] *Institute for Nuclear Theory, University of Washington, Seattle WA 98195-1550, U.S.A.*
[e] *Institute of Particle and Nuclear Physics, Faculty of Mathematics and Physics, Charles University in Prague, V Holešovičkách 2, 180 00 Praha 8, Czech Republic*
[f] *Theoretical Division, Los Alamos National Laboratory, Los Alamos, NM 87545, U.S.A.*

E-mail: s.elmorabit2@uva.nl, ryan.bouabid@duke.edu, cirigv@uw.edu, j.devries4@uva.nl, lukas.graf@nikhef.nl, emereghetti@lanl.gov

Abstract: We investigate two-neutrino double beta decay ($2\nu\beta\beta$) in chiral effective field theory. We find contributions from weak magnetism and double-weak pion-exchange at next-to-leading-order in the chiral power counting. We discuss the impact of the chiral corrections on the electron spectra and find that they should be included in analyses of $2\nu\beta\beta$ decay that aim to uncover new physics signatures in the electron spectrum. We illustrate this point by revisiting the effect of sterile neutrinos and non-standard charged interactions. We also find that the pion-exchange contributions involve nuclear matrix elements that are related to those appearing in neutrinoless double beta decay ($0\nu\beta\beta$). We investigate whether the $0\nu\beta\beta$ nuclear matrix elements can be obtained from detailed measurements of the energy spectrum of the outgoing electrons in $2\nu\beta\beta$ transitions.

Keywords: Effective Field Theories of QCD, Rare Decays, Baryon/Lepton Number Violation, Neutrino Interactions

ArXiv ePrint: 2412.14160

Open Access, © The Authors.
Article funded by SCOAP[3].

https://doi.org/10.1007/JHEP06(2025)082

JHEP06(2025)082

Contents

1 Introduction 1

2 The $2\nu\beta\beta$ amplitude and differential decay rate 2

3 The lepton energy expansion 8
3.1 Validation of the expansion method and the role of nuclear uncertainties 10

4 A sensitivity study of the spectrum 12

5 Beyond-the-standard-model contributions to $2\nu\beta\beta$ 15
5.1 $2\nu\beta\beta$ with sterile neutrinos 15
5.2 Non-standard charged-current interactions 17

6 Conclusion 19

1 Introduction

Double-weak processes, where two nucleons undergo β-decay and produce two (anti)neutrinos and two electrons ($2\nu\beta\beta$), are the slowest processes ever measured [1, 2]. For example, the lifetime of ^{76}Ge is 10^{21} yr, a staggering eleven orders of magnitude longer than the age of the universe [3]. A counterpart to $2\nu\beta\beta$ is the hypothetical *neutrinoless* double beta decay ($0\nu\beta\beta$), which involves the same transition, but without final-state neutrinos. The detection of $0\nu\beta\beta$ is one of the major goals for nuclear and particle physics in the coming decades [4, 5]. A signal of the process where two electrons are created without accompanying anti-neutrinos would prove that lepton number is not conserved in nature and demonstrate that neutrinos, unlike any other fermions in the Standard Model (SM), are Majorana particles. The most stringent limit on $0\nu\beta\beta$, $T^{0\nu}_{1/2}(^{136}\text{Xe}) > 3.8 \cdot 10^{26}$ yr (90% C.L.), was established earlier this year by the KamLAND-Zen collaboration [6], and next-generation experiments will have sensitivity to half-lives in excess of 10^{28} yr [5].

The development of modern $0\nu\beta\beta$ and dark-matter direct detection experiments has led to experiments with very large masses and extended data collection periods. New $0\nu\beta\beta$ and direct dark matter detection experiments will measure an unprecedented number of $2\nu\beta\beta$ events with very low background and can thus measure the electron energy spectrum with high precision [5, 7–10]. While $2\nu\beta\beta$ forms a background for $0\nu\beta\beta$, the $2\nu\beta\beta$ electron spectrum has been used both as a test for nuclear structure calculations [11, 12] as well as a tool to probe physics beyond the Standard Model (BSM) [13–28]. Using the $2\nu\beta\beta$ measurements in such a way requires an accurate theoretical description of the electron spectrum. A lot of effort has gone into electromagnetic corrections to the spectrum [29–31] and the effect of the outgoing lepton energy on the nuclear matrix elements [11].

In this work, we focus on a different type of correction associated with the form of the weak currents and more generally weak transition operators. The use of chiral EFT (χEFT) [32],

JHEP06(2025)082

the low-energy EFT of QCD that describes interactions of nucleons and pions, has proven very valuable in the description of $0\nu\beta\beta$ decay [33–35]. Here we apply the EFT framework to $2\nu\beta\beta$ decay and use χEFT to organize corrections to the $2\nu\beta\beta$ spectrum in a systematic expansion in the ratio of scales involved in the problem. We find two main corrections that should be included in the analysis of $2\nu\beta\beta$ spectra in order to isolate BSM physics:

- The first correction arises from the subleading one-nucleon contributions associated with weak magnetism (see related work in ref. [29, 36]). These are the first corrections in a multipole expansion of the weak currents, and affect the spectral shape at the per-mille level.

- A second type of correction arises from two-nucleon weak currents induced by pion exchange, along with the associated short-range two-nucleon operators needed to renormalize the amplitudes. We will show that these pion-induced chiral corrections to the $2\nu\beta\beta$ electron spectrum depend on nuclear matrix elements (NMEs) that also appear in the description of $0\nu\beta\beta$ induced by massive Majorana neutrino exchange.

A key problem in interpreting the results of $0\nu\beta\beta$ searches (null so far) is the theoretical prediction of the NMEs that suffer from an uncertainty up to an order of magnitude. Recent developments using χEFT and *ab initio* nuclear many-body calculations have been used to reduce this uncertainty, but a more direct approach to the NMEs would be very welcome. In this light, there have been attempts to find correlations between $0\nu\beta\beta$ NMEs and other observables like ion double-charge exchange [37–39], double Gamow-Teller matrix elements [40–42], nucleon-nucleon phase shifts [43], or double-magnetic dipole transitions [44, 45]. Although these studies are important and might reveal deficiencies in the many-body methods used to compute nuclear wavefunctions and matrix elements, these correlations are determined mainly phenomenologically and lack a precise theoretical understanding, i.e., in terms of matrix elements of the same two-body operator appearing in $0\nu\beta\beta$. The χEFT or low-energy QCD relation we find here is much more concrete and has a firm theoretical basis.

This paper is organized as follows. In section 2 we derive the $2\nu\beta\beta$ amplitude, including higher-order corrections in the chiral counting. To separate phase-space integrations from NMEs we discuss the lepton energy expansion introduced in ref. [11], in section 3, and verify it using different nuclear methods. We discuss how chiral corrections affect the $2\nu\beta\beta$ spectrum and the role of nuclear uncertainties in section 4. We compare the chiral corrections identified in this work to representative BSM corrections to the spectrum in section 5. We summarize, conclude, and present an outlook in section 6.

2 The $2\nu\beta\beta$ amplitude and differential decay rate

We consider the process

$$0^+(E_i) \to 0^+(E_f) + e^-(E_{e1}) + e^-(E_{e2}) + \bar{\nu}_e(E_{\nu 1}) + \bar{\nu}_e(E_{\nu 2})\,, \tag{2.1}$$

where $0^+(E_i)$ and $0^+(E_f)$ denote the initial- and final-state atomic ground states with vanishing total angular momentum and positive parity. The dominant contribution to this

JHEP06(2025)082

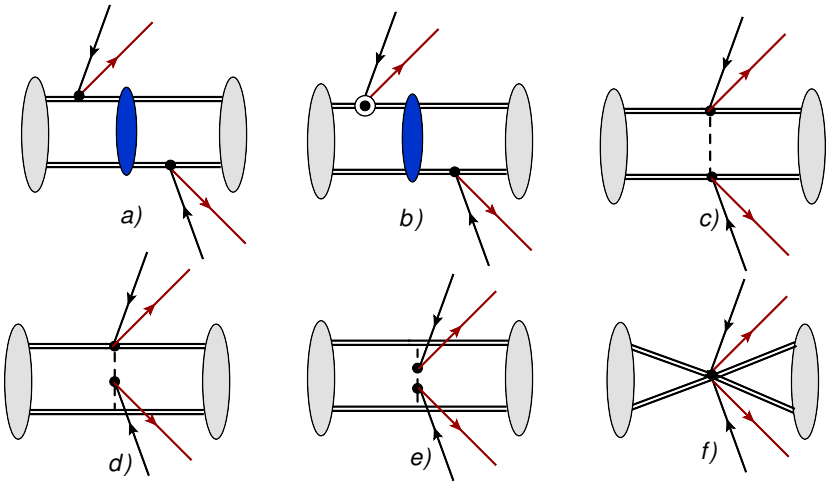

Figure 1. Diagrams contributing to $2\nu\beta\beta$. Gray ellipses denote the initial- and final-state nuclear wave functions, whereas the blue ellipse denotes strong interactions among intermediate nucleons that generate nuclear excited states. The LO diagram (a) describes two nucleons (double lines) undergoing β-decay into an electron (red lines) and anti-neutrinos (single black lines) through LO weak vertices (black dots). Diagram (b) involves a subleading β-decay vertex from weak magnetism. Diagrams (c)-(e) correspond to pion-exchange double-weak currents (pions are denoted by dashed lines). Finally diagram (f) describes a double-weak contact term that renormalizes diagrams (c)-(e).

decay arises from diagram (a) in figure 1. This contribution is very well studied in the literature and its amplitude can be written as [11, 29, 46]

$$T_{\beta\times\beta} = -\frac{4g_A^2 G_F^2 V_{ud}^2}{3m_e}\left(M_{GT}^K L_{11}^i L_{22}^i - M_{GT}^L L_{12}^i L_{21}^i\right) \tag{2.2}$$

in terms of the Fermi constant G_F, the nucleon axial charge $g_A \simeq 1.27$, and the CKM element $V_{ud} = 0.974$. We define the lepton current $L_{ij}^\mu = \bar{e}_L(p_{e,i})\gamma^\mu \nu_L(p_{\nu,j})$ and the dimensionless structures

$$M_{GT}^{K,L} = m_e \sum_n G_n \frac{E_n - \frac{1}{2}(E_i + E_f)}{[E_n - \frac{1}{2}(E_i + E_f)]^2 - \epsilon_{K,L}^2}\,, \tag{2.3}$$

where we encounter the nuclear matrix element associated to a double Gamow-Teller (GT) transition

$$G_n = \langle f|\sum_k \vec{\sigma}_k \tau_k^+ |n\rangle \cdot \langle n|\sum_l \vec{\sigma}_l \tau_l^+ |i\rangle\,, \tag{2.4}$$

where k, l sum over the nucleons inside the nucleus and n denotes an intermediate nuclear state with quantum number $J^\pi = 1^+$ and energy E_n. In addition, we introduced the combination of lepton energies

$$\epsilon_K = (E_{22} - E_{11})/2\,, \qquad \epsilon_L = (E_{12} - E_{21})/2\,, \tag{2.5}$$

in terms of $E_{ij} = E_{ei} + E_{\nu j}$. We have neglected a double Fermi NME in eq. (2.2) because it is suppressed by isospin breaking.

JHEP06(2025)082

Eqs. (2.2), (2.3) and (2.4) are nothing but the leading contributions in a multipole and chiral expansions, which can be organized in a double expansion in the small parameters ϵ_π and ϵ_χ, with

$$\epsilon_\chi = \mathcal{O}\left(\frac{k_F}{\Lambda_\chi}\right), \qquad \epsilon_\pi = \mathcal{O}\left(\frac{\mathcal{Q}}{k_F}\right), \tag{2.6}$$

where here by k_F we denote scales of the order of the typical momentum of nucleons inside nuclei, $k_F \sim m_\pi \sim 100\,\text{MeV}$, while $\mathcal{Q}$ denote the reaction's $\mathcal{Q}$-value, $\mathcal{Q} \sim E_{1,2} \sim m_e \sim$ few MeVs. We can roughly divide higher order contributions into 2 classes. In the first class we encounter diagram 1(b) with an intermediate nuclear state such as in diagram 1(a) but with subleading weak currents or with higher order terms in the lepton momenta. The nuclear matrix element in eq. (2.3) can be replaced by the more general expression

$$\begin{aligned} M^K = \frac{m_e}{g_A^2}\sum_n \Bigg(& \frac{1}{E_n - \frac{1}{2}(E_i+E_f) - \epsilon_K} \langle f| \sum_k \vec{J}_{V-A}(\vec{q}_{11})|n\rangle \cdot \langle n|\vec{J}_{V-A}(\vec{q}_{22})|i\rangle \\ & + \frac{1}{E_n - \frac{1}{2}(E_i+E_f) + \epsilon_K} \langle f| \sum_k \vec{J}_{V-A}(\vec{q}_{22})|n\rangle \cdot \langle n|\vec{J}_{V-A}(\vec{q}_{11})|i\rangle \Bigg), \end{aligned} \tag{2.7}$$

with $\vec{q}_{ij} = \vec{p}_{ei} + \vec{p}_{\nu j}$, and M^L can be obtained by replacing $\epsilon_K \to \epsilon_L$, $\vec{q}_{11} \to \vec{q}_{12}$ and $\vec{q}_{22} \to \vec{q}_{21}$. At zero lepton momentum, the leading corrections come from two-body axial currents. These scale as $\mathcal{O}\left(\epsilon_\chi^2\right)$, but amount to a shift in the total rate and do not affect the energy spectrum. At non-zero lepton momentum, the nuclear matrix elements in eq. (2.7) can be expanded by using the multipole expansion [47, 48]. This yields an expansion in $\mathcal{Q}/k_F$ or $\mathcal{Q}/m_N$, with m_N the nucleon mass, and in general affects both the total rate and the shape of the electron energy distribution. The leading contribution in the multipole expansion arises from weak magnetism (WM), at $\mathcal{O}(\mathcal{Q}/\Lambda_\chi) \sim 10^{-3}$. At $\mathcal{O}(\mathcal{Q}^2/k_F^2) \sim 10^{-4}$ one would find contributions from the induced pseudoscalar form factor, from the radii of the axial form factor, etc. We will focus here on the contribution from WM which is introduced through perturbing the nuclear current with a vectorial term proportional to g_M

$$J_N^\mu = g_V v^\mu - 2 g_A S^\mu + \left[\frac{i g_M}{m_N}\epsilon^{\mu\nu\alpha\beta} v_\alpha S_\beta q_\nu\right], \tag{2.8}$$

where $g_M = 1 + \kappa_1 = 4.7$ is the magnetic coupling, $v^\mu = \left(1, \vec{0}\right)$ and $S^\mu = \left(0, \frac{1}{2}\vec{\sigma}\right)$ are the nucleon velocity and spin.

In the second class of corrections we encounter diagrams 1(c)-(e) which involve an irreducible double-β two-nucleon transition. By power counting these diagrams, we can see that they are suppressed by $\mathcal{O}(\mathcal{Q}/\Lambda_\chi)$ with respect to the leading-order contributions. As for WM, these corrections do affect the electron spectrum. As the typical pion momentum $|\vec{q}|$ is of order k_F, and much larger than the electron and neutrino energies, these diagrams generate "neutrino potentials", analogous to those found in $0\nu\beta\beta$. Their contribution to $2\nu\beta\beta$ only depends on the initial and final state wavefunctions and not on the intermediate nuclear states. As a consequence, the amplitude does not contain the energy denominators in eqs. (2.3) and (2.7), and gives rise to a different dependence on the electron energy compared to the LO diagrams.

JHEP06(2025)082

Finally, we encounter diagram 1(f) that involves a double-weak contact interaction between four-nucleons and four-leptons that is necessary to renormalize diagrams 1(c)-(e) and, similarly, do affect the electron spectrum.

We now turn to the actual computation. The sum of irreducible diagrams (c)-(e) in figure 1 contribute to the double-weak two-nucleon transition operator (we will call it the two-neutrino potential) which can be computed using the LO χEFT Lagrangian (see e.g. ref. [49]). In momentum space the two-neutrino potential from diagrams (c)-(e) reads

$$V_{2\nu}(\vec{q}) = -\frac{(8G_F^2 V_{ud}^2)}{2F_\pi^2}(\tau_1^+\tau_2^+)\frac{1}{\vec{q}^2+m_\pi^2}\left(L_{11}^\mu L_{22}^\nu - L_{12}^\mu L_{21}^\nu\right)\left\{g_V^2\delta^{\mu 0}\delta^{\nu 0} + \frac{g_A^2}{3}\delta^{\mu i}\delta^{\nu i}\right.$$
$$\left.\times\left[\vec{\sigma}_1\cdot\vec{\sigma}_2\left(1+\frac{4}{3}\frac{\vec{q}^2}{\vec{q}^2+m_\pi^2}+\frac{4}{3}\left(\frac{\vec{q}^2}{\vec{q}^2+m_\pi^2}\right)^2\right)-\frac{4}{3}S_{12}\frac{\vec{q}^2}{\vec{q}^2+m_\pi^2}\left(1+\frac{\vec{q}^2}{\vec{q}^2+m_\pi^2}\right)\right]\right\} \tag{2.9}$$

in terms of $\vec{q}$, the momentum transfer between nucleon 1 and 2 and we have neglected the lepton momenta. The tensor operator is defined as $S_{12} = \vec{\sigma}_1\cdot\vec{\sigma}_2 - 3\vec{\sigma}_1\cdot\vec{q}\,\vec{\sigma}_2\cdot\vec{q}/\vec{q}^2$. The two-neutrino potentials are of pion range and have a Coulomb-like scaling for large virtual momenta $|\vec{q}| \gg m_\pi$. Their matrix elements on leading-order chiral wavefunctions therefore depend logarithmically on the ultraviolet cut-off used to regulate the short-range nuclear force. Similar divergences were observed in the case of the pion exchange potential [50], of pion-nucleus scattering operators [51, 52] and for the leading-order neutrino potential in $0\nu\beta\beta$ [33, 53], and can be cured by including short-range $2\nu\beta\beta$ operators at the same order as the contributions in eq. (2.9). These will yield a short-range potential

$$V_{2\nu}^S(\vec{q}) = -\frac{(8G_F^2 V_{ud}^2)}{2F_\pi^4}(\tau_1^+\tau_2^+)\left(L_{11}^\mu L_{22}^\nu - L_{12}^\mu L_{21}^\nu\right)\left(g_{2\nu,\mathrm{F}}^{\mathrm{NN}}\,\delta^{\mu 0}\delta^{\nu 0} - g_{2\nu,\mathrm{GT}}^{\mathrm{NN}}\,\delta^{\mu i}\delta^{\nu i}\right), \tag{2.10}$$

with

$$g_{2\nu,\mathrm{F}}^{\mathrm{NN}} \sim g_{2\nu,\mathrm{GT}}^{\mathrm{NN}} = \mathcal{O}(1). \tag{2.11}$$

The Gamow-Teller low-energy constant (LEC), $g_{2\nu,\mathrm{GT}}^{\mathrm{NN}}$, is related to the contact contribution to the isotensor axial polarizability introduced in refs. [54, 55]. We refrain here from writing down the complete set of chiral invariant operators that lead to eq. (2.10), but notice that chiral symmetry relates some of them to the pion-nucleus scattering operators introduced in ref. [52].

The two-neutrino potentials contribute to the Fourier-transformed amplitude through

$$T_{\beta\beta} = \langle f|\sum_{m,n}\int\frac{d^3q}{(2\pi)^3}e^{i\vec{q}\cdot\vec{r}}V_{2\nu}(\vec{q})|i\rangle\,, \tag{2.12}$$

where m, n sums over all nucleons in the nucleus. We write this more explicitly as

$$T_{\beta\beta} = -\frac{(8G_F^2 V_{ud}^2)}{m_e}\left[\epsilon_F\left(L_{11}^0 L_{22}^0 - L_{12}^0 L_{21}^0\right) + \epsilon_{GT}\left(L_{11}^i L_{22}^i - L_{12}^i L_{21}^i\right)\right], \tag{2.13}$$

where

$$\epsilon_F = \frac{m_e g_V^2}{2F_\pi^2}\frac{1}{4\pi R_A}\left(M_F(m_\pi) + \frac{m_\pi^2}{F_\pi^2}g_{2\nu,\mathrm{F}}^{\mathrm{NN}}\,M_{F,\,sd}\right) \tag{2.14}$$

$$\epsilon_{GT} = \frac{m_e g_A^2}{6F_\pi^2}\frac{1}{4\pi R_A}\left(M_{GT}^{AA}(m_\pi) - 2M_{GT}^{AP}(m_\pi) + 4M_{GT}^{PP}(m_\pi) - \frac{3m_\pi^2}{g_A^2 F_\pi^2}g_{2\nu,\mathrm{GT}}^{\mathrm{NN}}\,M_{F,\,sd}\right). \tag{2.15}$$

JHEP06(2025)082

The nuclear matrix elements are defined through

$$M_{F,(sd)}(m_\pi) = \langle 0^+| \sum_{m,n} h_{F,(sd)}(r, m_\pi)\tau_m^+\tau_n^+|0^+\rangle\,,$$
$$M_{GT}^{ab}(m_\pi) = \langle 0^+| \sum_{m,n} h_{GT}^{ab}(r, m_\pi)\vec{\sigma}_m\cdot\vec{\sigma}_n\tau_m^+\tau_n^+|0^+\rangle\,, \tag{2.16}$$

where $ab = \{AA, AP, PP\}$ and the radial functions are given by[1]

$$h_F(r, m_\pi) = \frac{2R_A}{\pi}\int_0^\infty dq \frac{q^2}{q^2+m_\pi^2} h_F(q^2)\frac{\sin qr}{qr}\,, \tag{2.17}$$
$$h_{F,sd}(r) = \frac{2R_A}{\pi m_\pi^2}\int_0^\infty dq q^2 h_F(q^2)\frac{\sin qr}{qr}\,, \tag{2.18}$$
$$h_{GT}^{ab}(r, m_\pi) = \frac{2R_A}{\pi}\int_0^\infty dq \frac{q^2}{q^2+m_\pi^2} h_{GT}^{ab}(q^2)\frac{\sin qr}{qr}\,, \tag{2.19}$$

in terms of

$$h_F(q^2) = h_{GT}^{AA}(q^2) = 1\,, \quad h_{GT}^{AP}(q^2) = -\frac{2}{3}\frac{q^2}{q^2+m_\pi^2}\,, \quad h_{GT}^{PP}(q^2) = \frac{1}{3}\frac{q^4}{(q^2+m_\pi^2)^2}\,. \tag{2.20}$$

By power counting we observe that $\epsilon_F \sim \epsilon_{GT} = \mathcal{O}(m_e/(4\pi F_\pi)) = \mathcal{O}(m_e/\Lambda_\chi) \simeq 0.1\%$. In eq. (2.13) we neglect tensor operators, whose matrix elements are typically significantly smaller than those of Fermi and Gamow-Teller operators [57–59].

The NMEs entering $\epsilon_{F,GT}$ very closely resemble those appearing in the description of $0\nu\beta\beta$. $0\nu\beta\beta$ induced by the exchange of light Majorana neutrinos involves $M_F(0)$ and $M_{GT}^{ab}(0)$. However, $0\nu\beta\beta$ induced by heavier sterile neutrinos does involve the required $M_F(m_\pi)$ and $M_{GT}^{ab}(m_\pi)$ and detailed calculations [60–64] of these NMEs have appeared. The ratios $M_F(m_\pi)/M_F(0)$ and $M_{GT}^{ab}(m_\pi)/M_{GT}^{ab}(0)$ are rather stable with respect to the applied nuclear many-body method and show a much smaller spread than the values for $M_F(0)$ and $M_{GT}^{ab}(0)$ themselves as shown in table 1, implying that an extraction of the NMEs evaluated at m_π provides information about the $0\nu\beta\beta$ NMEs. At the moment, given the unknown low-energy constants $g_{2\nu,\mathrm{F}}^{\mathrm{NN}}$ and $g_{2\nu,\mathrm{GT}}^{\mathrm{NN}}$, such a program cannot be carried out. On a related point, since we do not control the LECs $g_{2\nu,\mathrm{F}}^{\mathrm{NN}}$ and $g_{2\nu,\mathrm{GT}}^{\mathrm{NN}}$ we will not include them in our numerical analysis and we can only provide an incomplete estimate the size of the pion-exchange corrections to $2\nu\beta\beta$ observables.

The total amplitude at this order becomes

$$\begin{aligned} T_{\beta\times\beta} + T_{\beta\beta} = -\frac{(8G_F^2V_{ud}^2)}{m_e}\Bigg\{\frac{g_A^2}{6}\Bigg[\left(\left(M_{GT}^K + \frac{6\epsilon_{GT}}{g_A^2}\right)\delta_{ij} + \frac{ig_M}{2g_Am_N}(p_{11}-p_{22})^k\,\epsilon_{ijk}M_{GT}^K\right)L_{11}^iL_{22}^j \\ + \left(\left(M_{GT}^L + \frac{6\epsilon_{GT}}{g_A^2}\right)\delta_{ij} + \frac{ig_M}{2g_Am_N}(p_{12}-p_{21})^k\,\epsilon_{ijk}M_{GT}^L\right)L_{12}^iL_{21}^j\Bigg] \\ + \epsilon_F\left(L_{11}^0L_{22}^0 - L_{12}^0L_{21}^0\right)\Bigg\}\,, \end{aligned} \tag{2.21}$$

[1]The integral in eq. (2.18) is formally divergent, and should be interpreted as a regularization of the $\delta^{(3)}(r)$ function. Eq. (2.18) can be regulated in many ways, e.g. by adding a vector form factor, see eq. (30) in ref. [56].

JHEP06(2025)082

NMEs	^{76}Ge		^{136}Xe	
	QRPA	Shell Model	QRPA	Shell Model
$M_{GT}^{(-1)}$	0.069	0.058	0.010	0.013
ξ_{31}	0.10	0.13	0.39	0.17
ξ_{51}	0.017	0.022	0.12	0.046
$M_F(m_\pi)$	−1.16	−0.42	−0.56	−0.38
$M_{GT}^{AA}(m_\pi)$	3.57	1.91	2.03	1.55
$M_{GT}^{AP}(m_\pi)$	−1.47	−0.66	−0.83	−0.56
$M_{GT}^{PP}(m_\pi)$	0.50	0.22	0.29	0.19
$M_{F,\,sd}$	−3.46	−1.46	−1.53	−1.28
$M_F(m_\pi)/M_F(0)$	0.67	0.71	0.63	0.70
$M_{GT}^{AA}(m_\pi)/M_{GT}^{AA}(0)$	0.67	0.61	0.64	0.63
$M_{GT}^{AP}(m_\pi)/M_{GT}^{AP}(0)$	0.73	0.71	0.70	0.72
$M_{GT}^{PP}(m_\pi)/M_{GT}^{PP}(0)$	0.75	0.73	0.73	0.75
$M_{GT}(m_\pi)/M_{GT}(0)$	0.71	0.66	0.68	0.68
$\Delta_0 - 1$	0.040	0.020	0.14	0.077
$\Delta_2 - 1$	0.025	0.014	0.076	0.043

Table 1. Values of $2\nu\beta\beta$ and $0\nu\beta\beta$ NMEs computed in the quasi particle random phase approximation and nuclear shell model for ^{76}Ge and ^{136}Xe. The QRPA estimates of M_{GT}^{-1}, ξ_{31} and ξ_{51} are obtained from ref. [11], while the NSM values are calculated using the matrix elements in ref. [64]. The $0\nu\beta\beta$ NMEs use the QRPA and NSM calculations of refs. [58] and [59], respectively. The value of $M_{GT}^{(-1)}$ corresponds to no quenching of g_A.

where $T_{\beta\times\beta}$ and $T_{\beta\beta}$ are defined, respectively, in eq. (2.2) and (2.12). We introduce $p_{ij} = (E_{ij}, \vec{p}_{ij})$ to describe the change in nucleon four-momentum q in terms of lepton four momenta.

The corresponding decay rate, accounting for $1/(2!\times 2!)$ for identical electrons and neutrinos, is given by

$$\Gamma = \frac{(G_F V_{ud})^4}{8\pi^7 m_e^2} \int_{m_e}^{E_i-E_f-m_e} dE_{e1} \int_{m_e}^{E_i-E_f-E_{e1}} dE_{e2} \int_0^{E_i-E_f-E_{e1}-E_{e2}} dE_{\nu 1} \times E_{e1} p_{e1} E_{e2} p_{e2} E_{\nu 1}^2 E_{\nu 2}^2 \times F(E_{e1}, Z_f) \times F(E_{e2}, Z_f) \times C_{2\nu}\,, \tag{2.22}$$

where we should interpret $E_{\nu 2} = (E_i - E_f - E_{11} - E_{e2})$ and

$$C_{2\nu} = \frac{g_A^4}{3}\Bigg\{ \left[(M_{GT}^K)^2 + (M_{GT}^L)^2 + M_{GT}^K M_{GT}^L\right] \times \left[1 - \frac{2g_M}{3m_N g_A}\left(\mathcal{Q} + 2m_e - (E_{e1}+E_{e2})\frac{2E_{e1}E_{e2} - m_e^2}{E_{e1}E_{e2}}\right)\right] + \frac{6}{g_A^2}\left(3\epsilon_{GT} - \epsilon_F\right)\left(M_{GT}^K + M_{GT}^L\right)\Bigg\} + \ldots \tag{2.23}$$

JHEP06(2025)082

Here $\mathcal{Q} = E_{11} + E_{22} - 2m_e$ and the dots denote higher-order terms. We have inserted the Fermi function

$$F(E,Z) = \left|\frac{2}{\Gamma(1+2\gamma_0)}\right|^2 (2pR)^{2(\gamma_0-1)} e^{\pi y} |\Gamma(\gamma_0 + iy)|^2 \,, \tag{2.24}$$

where $p = \sqrt{E^2 - m_e^2}$, $\gamma_0 = \sqrt{1 - Z^2\alpha^2}$, and $y = \alpha ZE/p$, to account for the leading Coulomb corrections [11]. This equation treats the nucleus as a point source, and it cures the divergence in the solution of the Dirac equation at $r = 0$ by evaluating the wavefunction at a somewhat arbitrary "nuclear radius", R. Typically R is chosen to be $R = 1.2A^{1/3}\,\text{fm}$ [30], or, in the superallowed β decay literature, $R = \sqrt{5/3}\langle r_{\text{ch}}^2\rangle^{1/2}$ [65, 66].

An EFT understanding of the Fermi function, its dependence on the nuclear scale R and the interplay with nuclear-structure-dependent matrix elements were presented in refs. [67–69]. The Fermi function in eq. (2.24) can be refined by including the effects of the nuclear charge distribution and electron screening, using for example the Thomas-Fermi approximation where one introduces an "effective" charge $Z \to Z_{\text{eff}}(r, Z)$. We use eq. (2.24) as our reference for the evaluation of phase space factors. Using the RADIAL Fortran package [70], we checked that we can reproduce the $2\nu\beta\beta$ phase space factors in ref. [11, 30], if we adopt the prescription in [30] and evaluate the electron wavefunctions at $r = R$. While finite size and screening effects change the phase space by about 10% [11], the effect on the normalized energy spectrum is about 0.1% in the full energy range. At this level of accuracy, other missing corrections, such as radiative corrections, affect the spectrum. We therefore limit ourselves to the simple function in eq. (2.24), but stress that future analyses should consider the theoretical error induced by missing electromagnetic corrections.

3 The lepton energy expansion

For computing observables we wish to factor out the leptonic component from the NME. Following ref. [11], we expand eq. (2.23) with respect to $[\epsilon_{K,L}/\tilde{A}]$, where $\tilde{A} = \left(E_n - \frac{1}{2}(E_i + E_f)\right)$ is the excitation energy with respect to the initial and final ground state.

$$M_{GT}^{K,L} = \sum_{m=0}^{\infty} M_{GT}^{(-2m-1)} \left(\frac{\epsilon_{K,L}}{2m_e}\right)^{2m} \,, \tag{3.1}$$

where $M_{GT}^{(-2m-1)}$ contains nuclear energies and matrix elements

$$M_{GT}^{(-2m-1)} = m_e (2m_e)^{2m} \sum_n \frac{G_n}{\tilde{A}^{2m+1}} \,. \tag{3.2}$$

In the next subsection we demonstrate that the lepton energy expansion converges rapidly. Expanding up to quartic terms we obtain

$$C_{2\nu} = g_A^4 \left[M_{GT}^{(-1)}\right]^2 \Delta_0 \left(\mathcal{A}_0 + \mathcal{A}_2\, \xi_{31} \frac{\Delta_2}{\Delta_0} + \mathcal{A}_4 \left(\xi_{51}\frac{\Delta_2}{\Delta_0} + \frac{1}{3}\xi_{31}^2\right) + \mathcal{A}_{22}\frac{1}{3}\xi_{31}^2 + \frac{\mathcal{A}_M}{\Delta_0}\right) + \dots \tag{3.3}$$

JHEP06(2025)082

where the dots denote higher-order terms. We have defined here the functions of lepton energies

$$\mathcal{A}_0 = 1\,, \qquad \mathcal{A}_2 = \frac{\epsilon_K^2+\epsilon_L^2}{(2m_e)^2}\,, \qquad \mathcal{A}_4 = \frac{\epsilon_K^4+\epsilon_L^4}{(2m_e)^4}\,, \qquad \mathcal{A}_{22} = \frac{\epsilon_K^2\epsilon_L^2}{(2m_e)^4}$$
$$\mathcal{A}_M = \frac{2g_M}{3m_N g_A}\frac{(E_{e1}+E_{e2})(2E_{e1}E_{e2}-m_e^2)}{E_{e1}E_{e2}}\,, \tag{3.4}$$

and the combination of hadronic and nuclear matrix elements

$$\xi_{31} = \frac{M_{GT}^{(-3)}}{M_{GT}^{(-1)}}\,, \qquad \xi_{51} = \frac{M_{GT}^{(-5)}}{M_{GT}^{(-1)}}\,,$$
$$\Delta_0 = 1 + \frac{4}{g_A^2}\frac{(3\epsilon_{GT}-\epsilon_F)}{M_{GT}^{(-1)}} - \frac{2g_M}{3m_N g_A}(\mathcal{Q}+2m_e)\,,$$
$$\Delta_2 = 1 + \frac{2}{g_A^2}\frac{(3\epsilon_{GT}-\epsilon_F)}{M_{GT}^{(-1)}}\,. \tag{3.5}$$

The WM and pionic corrections shift the overall decay rate through the factor Δ_0 but isolating this term is difficult due to the poor theoretical knowledge of the effective combination $g_A^4(M_{GT}^{(-1)})^2$. Furthermore, there are other terms at this order in the chiral expansion that modify the overall rate, such as, for example, two-body currents. The WM term will lead to corrections to the electron energy spectrum and we will discuss below how it can be isolated from the normalized differential decay rate. The pionic corrections are more difficult to isolate because the largest correction to the spectrum is degenerate with the ratio of NMEs ξ_{31}. While this ratio is significantly better known than the NMEs themselves, the uncertainty is still quite large. At $\mathcal{O}(\epsilon_{K,L}^4)$ we see further pionic corrections proportional to Δ_2/Δ_0.

The total decay rate can be calculated from

$$\frac{1}{\tau_{2\nu}} = \frac{\Gamma}{\ln 2} = g_A^4\left(M_{GT}^{(-1)}\right)^2\Delta_0\left[G_0^{2\nu} + \xi_{31}\frac{\Delta_2}{\Delta_0}G_2^{2\nu} + G_4^{2\nu}\left(\xi_{51}\frac{\Delta_2}{\Delta_0}+\frac{1}{3}\xi_{31}^2\right) + G_{22}^{2\nu}\frac{1}{3}\xi_{31}^2 + G_M^{2\nu}\right], \tag{3.6}$$

in terms of the phase space integrals

$$G_i^{2\nu} = \frac{1}{\ln 2}\frac{(G_F V_{ud})^4}{8\pi^7 m_e^2}\int_{m_e}^{E_i-E_f-m_e} dE_{e1}\int_{m_e}^{E_i-E_f-E_{e1}} dE_{e2}\int_0^{E_i-E_f-E_{e1}-E_{e2}} dE_{\nu 1}$$
$$\times E_{e1}p_{e1}E_{e2}p_{e2}E_{\nu 1}^2E_{\nu 2}^2 \times F(E_{e1},Z_f)\times F(E_{e2},Z_f)\times\mathcal{A}_i\,. \tag{3.7}$$

We often use a different set of kinematic variables and we define $\epsilon = E_{e1}+E_{e2}-2m_e$ and $\Delta = (E_{e1}-E_{e2})/2$ as the total electron kinetic energy and electron energy difference.We then write

$$G_i^{2\nu} = \frac{1}{\ln 2}\frac{(G_F V_{ud})^4}{8\pi^7 m_e^2}\int_0^{\mathcal{Q}} d\epsilon\int_{-\epsilon/2}^{\epsilon/2} d\Delta\int_0^{\mathcal{Q}-\epsilon} dE_{\nu 1}$$
$$\times E_{e1}p_{e1}E_{e2}p_{e2}E_{\nu 1}^2E_{\nu 2}^2 \times F(E_{e1},Z_f)\times F(E_{e2},Z_f)\times\mathcal{A}_i\,. \tag{3.8}$$

The differential decay rate becomes

$$\frac{d\Gamma}{d\epsilon} = g_A^4\left(M_{GT}^{(-1)}\right)^2\Delta_0\left[\frac{dG_0^{2\nu}}{d\epsilon} + \frac{dG_2^{2\nu}}{d\epsilon}\xi_{31}\frac{\Delta_2}{\Delta_0} + \frac{dG_4^{2\nu}}{d\epsilon}\left(\xi_{51}\frac{\Delta_2}{\Delta_0}+\frac{1}{3}\xi_{31}^2\right) + \frac{dG_{22}^{2\nu}}{d\epsilon}\frac{1}{3}\xi_{31}^2 + \frac{dG_M^{2\nu}}{d\epsilon}\right], \tag{3.9}$$

JHEP06(2025)082

where

$$\frac{dG_i^{2\nu}}{d\epsilon} = \frac{1}{\ln 2}\frac{(G_F V_{ud})^4}{8\pi^7 m_e^2}\int_{-\epsilon/2}^{\epsilon/2} d\Delta \int_0^{\mathcal{Q}-\epsilon} dE_{\nu 1} \times E_{e1} p_{e1} E_{e2} p_{e2} E_{\nu 1}^2 E_{\nu 2}^2 \times F(E_{e1}, Z_f) \times F(E_{e2}, Z_f) \times \mathcal{A}_i \,. \tag{3.10}$$

To factor out uncertainties in the overall NMEs, we consider the normalized differential decay rate (or the shape factor)

$$S(\epsilon) \equiv \frac{1}{\Gamma}\frac{d\Gamma}{d\epsilon}. \tag{3.11}$$

In what follows, we will compute $S_i^{(n)}(\epsilon)$, where the superscript (n) indicates the order of the $\epsilon_{K,L}^{2n}$ expansion, with $n \in \{0, 1, 2, \ldots\}$. A subscript is also added, $i \in \{0, WM, \pi, \chi\}$ which correspond to the uncorrected spectrum, the spectrum including only weak magnetism, only pion exchange, and both weak-magnetic and pionic corrections (chiral χ). For example, eq. (3.9) after normalization by the total rate corresponds to $S_\chi^{(2)}$.

3.1 Validation of the expansion method and the role of nuclear uncertainties

The lepton energy expansion method using QRPA matrix elements was introduced and discussed in detail in ref. [11]. We are interested in verifying the reliability of the expansion for the Nuclear Shell Model (NSM) and to assess the nuclear physics uncertainty on the $2\nu\beta\beta$ spectrum.

Ref. [64] presented nuclear shell-model calculations of the matrix elements for the transitions from the 0^+ ground states of ^{76}Ge and ^{76}Se into 1^+ states of the intermediate ^{76}As, and, analogously, for the transitions of ^{136}Xe and ^{136}Ba onto ^{136}Cs. Details of the calculations, and the values of the reduced matrix elements used are given in refs. [64, 71]. Shell-model calculations overestimate the Gamow-Teller matrix elements [72], and the effective Gamow-Teller matrix elements are obtained by multiplying the "bare" results in ref. [64] by a quenching factor q. The quenching factors have been estimated as $q_{^{76}\mathrm{Ge}} = 0.60$ and $q_{^{136}\mathrm{Xe}} = 0.45$ in ref. [73], or, more conservatively, to be in the ranges $q_{^{76}\mathrm{Ge}} = [0.55, 0.67]$ [71], $q_{^{136}\mathrm{Xe}} = [0.42, 0.57]$ [74]. Accounting for the quenching factors and using the phase space factors from ref. [11], the resulting $2\nu\beta\beta$ half-lives are

$$T_{2\nu}(^{76}\mathrm{Ge}) = [1.5, 3.3] \cdot 10^{21}\,\mathrm{yr}\,, \qquad T_{2\nu}(^{136}\mathrm{Xe}) = [0.6, 2.0] \cdot 10^{21}\,\mathrm{yr}\,, \tag{3.12}$$

compatible with the experimental results [3, 75]

$$T_{2\nu}(^{76}\mathrm{Ge}) = (2.022 \pm 0.042) \cdot 10^{21}\,\mathrm{yr}\,, \qquad T_{2\nu}(^{136}\mathrm{Xe}) = (2.165 \pm 0.061) \cdot 10^{21}\,\mathrm{yr}\,. \tag{3.13}$$

The nuclear uncertainty on the total rate is a factor of two to three and thus sizable.

To test the convergence of the epsilon expansion we first turn off the chiral and WM corrections and compare the unexpanded spectral shape $S(\epsilon)$ to $S^{(n)}(\epsilon)$ for $n = \{0, 1, 2, 3, \ldots\}$ in figure 2. We see convergence for both Ge and Xe, but to control the spectral shape at the per-mille level requires $n = 2$ corrections for ^{76}Ge and, in principle, $n = 3$ corrections for ^{136}Xe. Considering that the difference between $n = 3$ and $n = 2$ for ^{136}Xe is only relevant near the end-point of the spectrum, we will expand up to $n = 2$ in the rest of this work.

JHEP06(2025)082

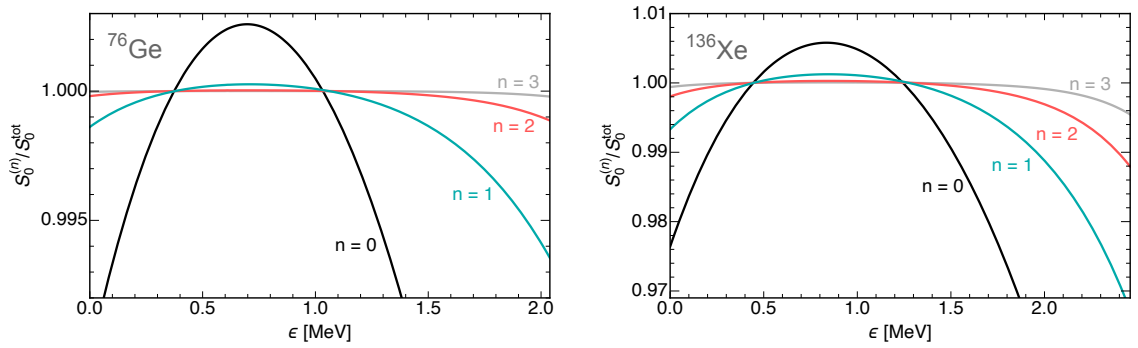

Figure 2. Convergence of the expansion for Ge (left) and Xe (right). We show the ratio of the expanded to the unexpanded shape factor, $S_0^{(n)}/S_0^{\rm tot}$, for order 0 (black), 1 (green), 2 (red), and 3 (gray). $S^{\rm tot_0}$ denotes the shape factor without expanding in lepton energies.

Each order in the lepton energy expansion is associated with new ratios of NMEs such as ξ_{31}. The uncertainty on these ratios will make it harder to identify the chiral, WM or BSM corrections on the $2\nu\beta\beta$ spectrum. Within the QRPA method the uncertainty on the NME ratios can be estimated by comparing the calculated ratios for different amount of g_A quenching [11]. For each effective g_A value, the amount of proton-neutron pairing in the Hamiltonian is adjusted to fit the $2\nu\beta\beta$ total rate, but this does not fix the values of the NME ratios. Using this variation, from the results presented in ref. [11] we obtain

$$\begin{aligned} ^{76}\text{Ge(QRPA)}: &\quad \xi_{31} = 0.11 \pm 0.01\,, &\quad \xi_{51} = 0.021 \pm 0.004\,, \\ ^{136}\text{Xe(QRPA)}: &\quad \xi_{31} = 0.32 \pm 0.06\,, &\quad \xi_{51} = 0.10 \pm 0.02\,, \end{aligned} \tag{3.14}$$

corresponding to 10%-20% nuclear uncertainty on the ratios.

This is only the uncertainty within a given nuclear many-body method. We would like to compare this to NME ratios obtained within the nuclear shell model. Using the NMEs obtained in ref. [64] we can compute the central values given in table 1. To assess the uncertainty we see how much the ratios vary if we change the individual transition matrix elements. We generate 5000 sets of matrix elements by multiplying each by a random number between 0.1 and 10, subjected to the restriction that the $2\nu\beta\beta$ half-life is within the range given in eq. (3.12). We then use this set to compute an average ξ_{ij}. We obtain

$$\begin{aligned} ^{76}\text{Ge(NSM)}: &\quad \xi_{31} = 0.12 \pm 0.02\,, &\quad \xi_{51} = 0.022 \pm 0.004\,, \\ ^{136}\text{Xe(NSM)}: &\quad \xi_{31} = 0.16 \pm 0.04\,, &\quad \xi_{51} = 0.042 \pm 0.012\,, \end{aligned} \tag{3.15}$$

finding 20%-30% uncertainties. We stress that this is just a rough estimate of the theoretical uncertainty. While the ^{76}Ge NME ratios are in good agreement with the QRPA results, the ^{136}Xe ratios are smaller by about a factor 2. The mismatch for ^{136}Xe indicates a disagreement between QRPA and the NSM regarding the importance of the low-energy excited states. An extraction of ξ_{31} from results of the KamLAND-Zen experiment showed that part of the range of ξ_{31} as predicted by the QRPA was partially excluded [12] but more data is necessary to draw a firmer conclusion. Below we will present results for the QRPA and NSM separately instead of attempting to combine the uncertainties from the two methods. We focus here

JHEP06(2025)082

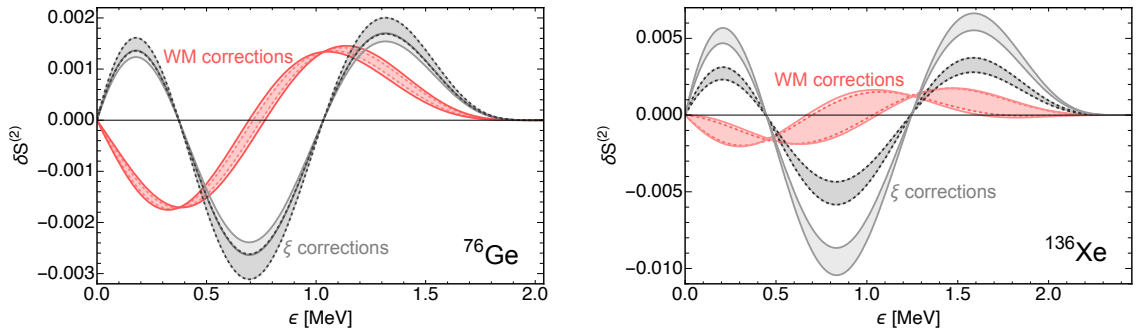

Figure 3. Effects of theoretical uncertainties on ξ_{31} and ξ_{51} on $\delta S^{(2)}$ for ^{76}Ge (left) and ^{136}Xe (right) in comparison with the effects of the correction induced by the weak magnetism term (red). We show results for both NSM (darker, dashed curves) and QRPA (lighter, solid curves).

on QRPA and NSM NMEs, but the discussion can be applied to other many-body methods. In particular, it would be interesting to apply the same *ab initio* methods used for $0\nu\beta\beta$ NMEs [35, 41, 43, 76] to $2\nu\beta\beta$, which might shed light on the issue of g_A quenching, and provide a validation of the calculations of ξ_{31} and ξ_{51}.

In figure 3 we show the resulting uncertainty on $\delta S_0^{(2)} \equiv (S_0^{(2)} - S_0^{(0)})$ due to the theoretical uncertainty on ξ_{31} and ξ_{51} for both QRPA and NSM. In particular, for ^{136}Xe the discrepancies in the NMEs between the QRPA and the NSM are worrying. However, at certain specific energies, the uncertainties become small because the dependence on ξ_{31} disappears. These nodes occur whenever

$$\frac{dG_2^{2\nu}}{d\epsilon} \simeq \frac{G_2^{2\nu}}{G_0^{2\nu}} \frac{dG_0^{2\nu}}{d\epsilon}\,, \tag{3.16}$$

which depends just on phase space factors and not on nuclear theory. The nodes are interesting places to find deviations from the predicted $2\nu\beta\beta$ spectrum. We illustrate this by depicting the effect of WM corrections in red. The WM effects are comparable to the ϵ corrections and distinguishable despite nuclear uncertainties, in particular for energies around the nodes. This explains the appearance of the common nodes in 2, with the approximate nuclear independence also appearing in the similarity between different isotopes in figure 5.

4 A sensitivity study of the spectrum

In this section, we discuss the quantitative impact of the chiral corrections on the (differential) decay rate. The total $2\nu\beta\beta$ rate is not precisely predicted by nuclear theory and suffers from a large theoretical uncertainty, as indicated in eq. (3.12). Nevertheless, it is interesting to study the impact of the chiral corrections on the total rate. To do so, we use the central value of $M_{GT}^{(-1)}$ and the ξ ratios as given in table 1. We give the resulting corrections to the lifetime in table 2. The chiral corrections on the lifetime are dominated by the pionic contributions and reduce the ^{76}Ge lifetime by a 2%-5% and of ^{136}Xe by 7%-13%. These shifts are sizable and indicate that it might be interesting to consider the remaining chiral corrections to the lifetime.

Corrections to the total rate are hard to isolate due to the large nuclear uncertainty. To quantify deviations on the shape factor we consider both the difference of spectra and

JHEP06(2025)082

	^{76}Ge QRPA	^{76}Ge NSM	^{136}Xe QRPA	^{136}Xe NSM
$T_0^{(2)}$	1.50	2.13	1.79	1.21
$T_\pi^{(2)}$	1.43	2.08	1.56	1.12
$T_{\rm WM}^{(2)}$	1.51	2.14	1.79	1.21
$T_\chi^{(2)}$	1.43	2.08	1.56	1.12

Table 2. Decay rates in units of 10^{21} yr with ($T_{i\neq 0}^{(2)}$) chiral and without ($T_0^{(2)}$) chiral corrections using eqs. (3.14) and (3.15). We have used $M_{GT}^{(-1)}$ and ξ values given in table 1.

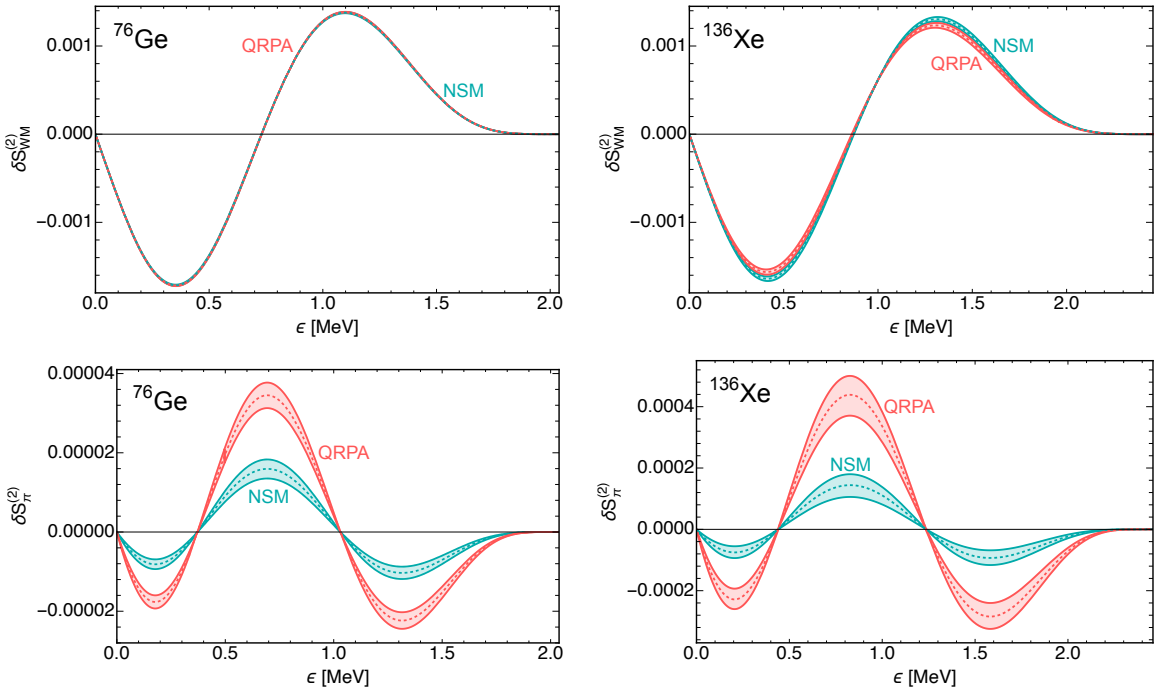

Figure 4. Distortion in the spectral shape due to weak magnetism term (upper panel) and pion corrections (lower panel) for Germanium (left) and Xenon (right) with the ξ_{31} and ξ_{51} parameters varied within the ranges given in eqs. (3.15) (NSM, depicted in blue) and in eqs. (3.14) (QRPA, depicted in red).

relative fraction:

$$\delta S_i^{(m)}(\epsilon) = S_i^{(m)}(\epsilon) - S_0^{(m)}(\epsilon)\,, \quad \delta \bar{S}_i^{(m)}(\epsilon) = \delta S_i^{(m)}(\epsilon)/S_0^{(m)}(\epsilon)\,. \tag{4.1}$$

Although easy to compute with the expressions given above, the interpretation in terms of measurable quantities requires careful thinking regarding nuclear uncertainties. We depict the distortion of the energy electron spectrum in figure 4. The width of the bands is obtained by varying ξ_{31} and ξ_{51} by their ranges specified in eqs. (3.14) and (3.15). It is important to stress that while we vary ξ's in this range we use the same value in both $S_0^{(m)}$ and $S_i^{(m)}$. That is, the uncertainty is correlated leading to rather thin bands in figure 4. The effect of WM on the ^{76}Ge and ^{136}Xe spectra is shown in the upper panel of figure 4. WM shifts

JHEP06(2025)082

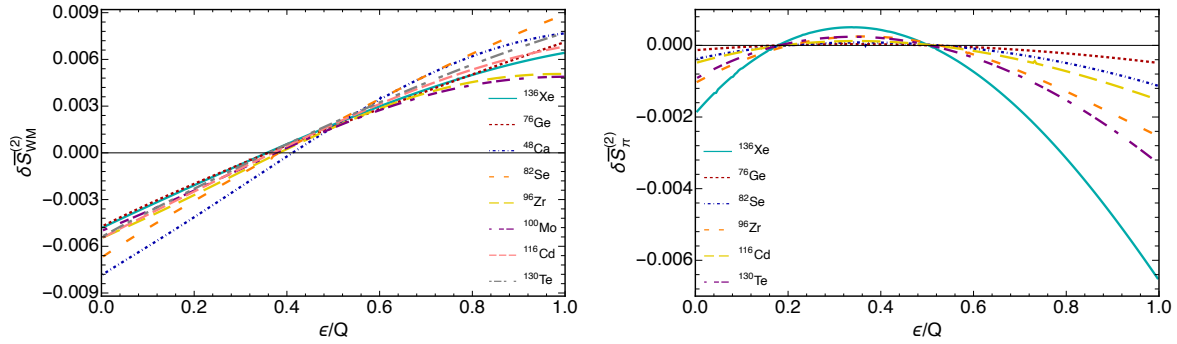

Figure 5. The weak-magnetic (left) and pionic (right) corrections to the normalized spectral shape for various isotopes.

the spectrum's peak to higher energies and causes few per-mille changes to the shape of the spectrum. The pion corrections, shown in the lower panel, modulate the shape, with enhancement at the center, attenuation at roughly two- and four-fifths of the spectrum, and nodes at the endpoints and in between the attenuation and enhancement. For ^{76}Ge the pionic corrections are very small, but they are comparable to WM for ^{136}Xe. However, the pionic corrections should only be seen as rough estimates as the short-distance contributions are not included and could change the overall size of the effect.

While we focus on ^{76}Ge and ^{136}Xe in this paper for brevity, the identified spectral distortions also appear for other isotopes that undergo $2\nu\beta\beta$. We show the WM and pionic corrections in the left and right panels of figure 5, respectively. We have used ξ values from ref. [11] and the $0\nu\beta\beta$ NMEs necessary to evaluate $\epsilon_{F,GT}$ from ref. [77], which used the QRPA calculation of ref. [58]. We have not included nuclear uncertainty bands to avoid cluttering the plot. The WM effects are fairly isotope independent, ranging from -0.7% to $+0.7\%$ over the energy range. The pionic corrections show a smaller variance for ^{76} Ge and ^{82} Se but a larger variance for heavier isotopes ^{130}Te and ^{136}Xe (up to -0.8% near the end point of the spectrum).

While this shape modulation is non-trivial, the uncertainty in the value of ξ_{31} and ξ_{51} complicates things. The extrema of the pionic corrections are washed out by the uncertainty in ξ_{31}, which are convolved with the pionic corrections via the product $\xi_{31}\Delta_2/\Delta_0$. To identify WM, chiral, or BSM corrections from accurate measurements of the spectrum, we either have to subtract $S_0(\epsilon)$ from the data and compare the resulting difference $\delta S_{\rm exp} = S_{\rm exp} - S_0$ with δS_i, or perform a joint fit to ξ_{31}, ξ_{51}, and the parameters in chiral corrections. The former procedure would add a theoretical error to $\delta S_{\rm exp}$. To model this theory error, and to assess whether the chiral corrections can be distinguished from the ξ corrections to the spectrum, we treat the ξs as independent normally distributed variables[2] in $S_i(\epsilon)$ and $S_0(\epsilon)$, and then compute the resulting uncertainty on $\delta S_i(\epsilon)$. This procedure is equivalent to considering $\delta S_i - \delta S_{\rm exp}$, with the assumption that experimental data have no error, and their central

[2]We assume that the ξs are uniformly distributed in the ranges specified by eqs. (3.14) and (3.15). We then compute the associated standard deviation for a normal distribution by taking the uniform spread divided by $\sqrt{12}$ to align the variance of the normal and uniform distribution. For example, for ^{76}Ge and the QRPA method we obtain $\sigma(\xi_{31}) = 0.02/\sqrt{12} = 0.0058$.

JHEP06(2025)082

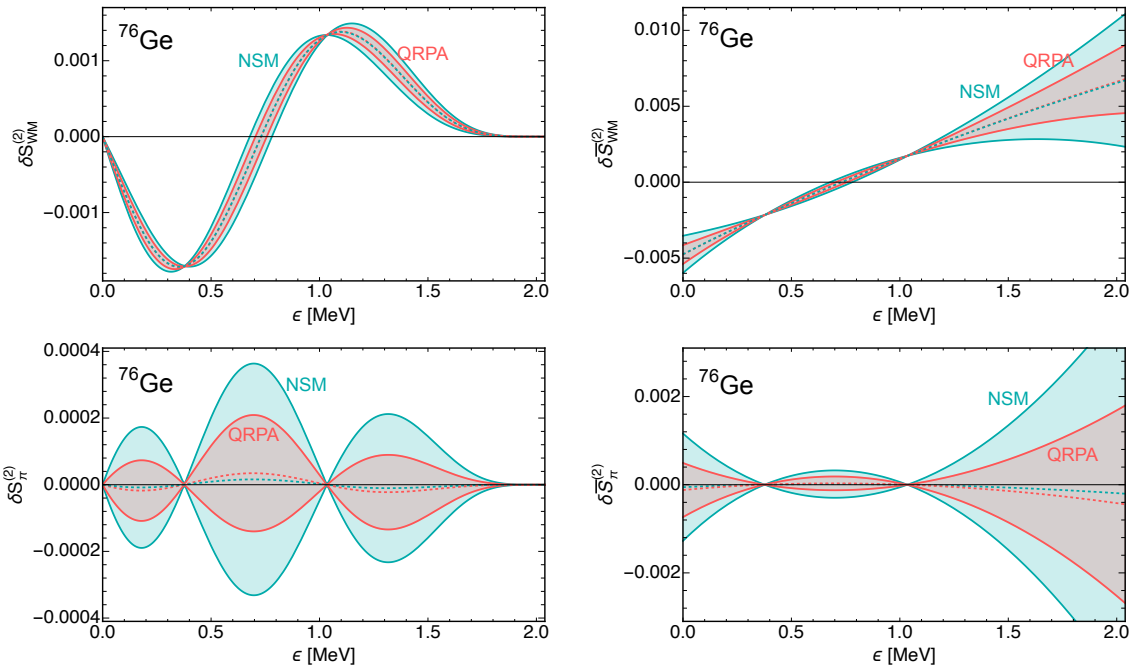

Figure 6. Top: absolute (left) and normalized (right) shift in the spectral shape due to WM (top) and pion (bottom) corrections for ^{76}Ge for QRPA (red) and NSM (blue) NMEs. The procedure to obtain the uncertainty bands is described in the main text.

value exactly agrees with $S_0(\epsilon)$, or $\delta S_{\rm exp} = 0$. If $\delta S_i(\epsilon)$ calculated in this way is incompatible with zero, it would indicate that the effect is not overwhelmed by the uncertainties on ξ, and thus observable, provided that the experimental measurements have comparable accuracy.

The resulting nuclear uncertainty is shown by the bands in figures 6, for ^{76}Ge, and 7 for ^{136}Xe. For both isotopes, the WM effects are still distinguishable, in particular for electron energies around the nodes identified in eq. (3.16). The pionic corrections are washed out with current ξ_{31}, ξ_{51} uncertainties and are unlikely to be measured without greater control of, in particular, ξ_{31}.

5 Beyond-the-standard-model contributions to $2\nu\beta\beta$

Considering the large amount of experimental activity in the field of $2\nu\beta\beta$, it would be interesting to use the measured electron spectra as a test of the SM. This has already been done to look for sterile neutrinos, majorons, and CPT violation [16, 17, 19, 20, 22–28]. In this section, we review how various BSM effects could modify the electron spectrum and how this compares to the chiral corrections identified above.

5.1 $2\nu\beta\beta$ with sterile neutrinos

One interesting possibility is that in $2\nu\beta\beta$ a so-called sterile neutrino is produced with a mass below the $\mathcal{Q}$-value of the reaction. In this case, the total measured differential decay

JHEP06(2025)082

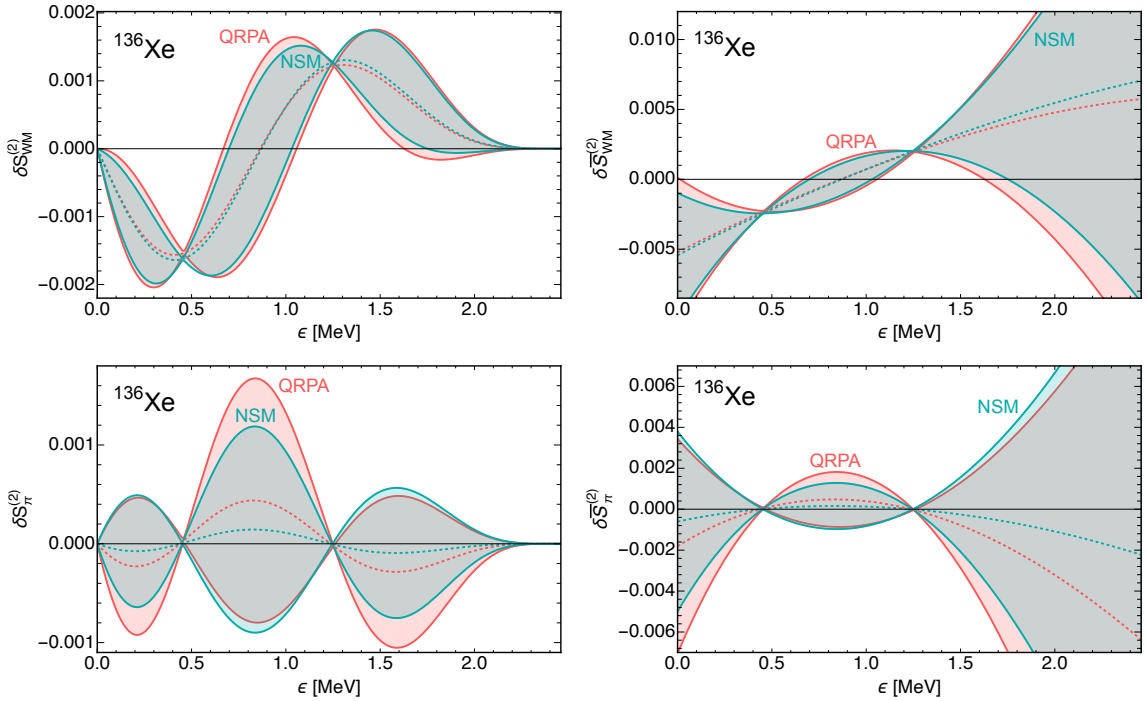

Figure 7. Top: absolute (left) and normalized (right) shift in the spectral shape due to WM (top) and pion (bottom) corrections for ^{136}Xe for QRPA (red) and NSM (blue) NMEs. The procedure to obtain the uncertainty bands is described in the main text.

rate is given by

$$\frac{d\Gamma^{2\nu}(m_N,|V_{eN}|)}{d\epsilon} = (1-|V_{eN}|^2)^2\frac{d\Gamma}{d\epsilon} + 2(1-|V_{eN}|^2)|V_{eN}|^2\,\frac{d\Gamma^{\nu N}(m_N)}{d\epsilon}\,, \tag{5.1}$$

in terms of the mass of the sterile neutrino m_N and the mixing angle V_{eN}. The rate $\Gamma^{\nu N}$ is defined for the process where a light and a sterile neutrino is produced. It can be calculated from

$$\frac{\Gamma^{\nu N}}{\ln 2} = g_A^4\left(M_{GT}^{(-1)}\right)^2\left[G_0^{\nu N}+\xi_{31}G_2^{\nu N}+G_4^{\nu N}\left(\xi_{51}+\frac{1}{3}\xi_{31}^2\right)+G_{22}^{\nu N}\frac{1}{3}\xi_{31}^2\right]\,, \tag{5.2}$$

where the phase space integrals are now defined as

$$\begin{aligned} G_i^{\nu N} = \frac{1}{\ln 2}\frac{(G_F V_{ud})^4}{8\pi^7 m_e^2}\int_0^{\mathcal{Q}-m_N} d\epsilon \int_{-\epsilon/2}^{\epsilon/2} d\Delta \int_{m_N}^{\mathcal{Q}-\epsilon} dE_N \\ \times E_{e1}p_{e1}E_{e2}p_{e2}E_{\nu 1}^2 E_N\sqrt{E_N^2-m_N^2}\times F(E_{e1},Z_f)\times F(E_{e2},Z_f)\times A_i\,, \end{aligned} \tag{5.3}$$

where $E_{\nu 1}=(E_i-E_f-E_{e1}-E_{e2}-E_N)$ is implied. We define the shape factor as

$$S_N(\epsilon) = \frac{1}{\Gamma^{2\nu}(m_N,|V_{eN}|)}\frac{d\Gamma^{2\nu}(m_N,|V_{eN}|)}{d\epsilon}\,. \tag{5.4}$$

As an example we depict

$$\delta S_N(\epsilon) = S_N(\epsilon) - S_0(\epsilon)\,, \tag{5.5}$$

JHEP06(2025)082

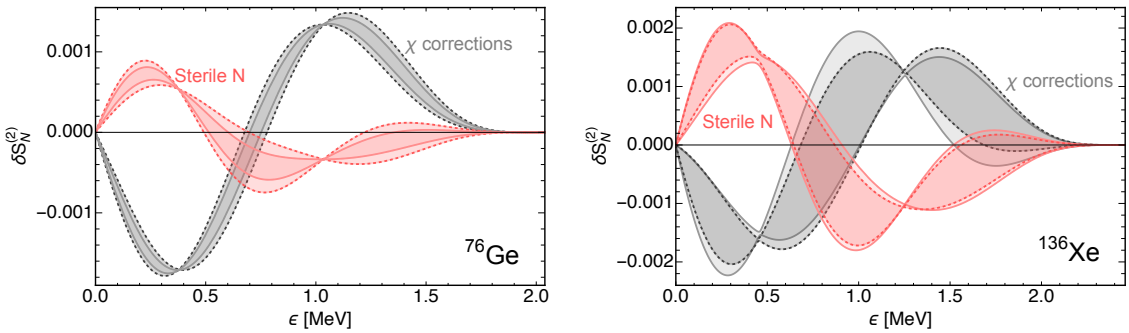

Figure 8. Shape-factor deviations δS_N stemming from the chiral corrections in comparison with deviations introduced by a hypothetical sterile-neutrino contribution with mass $M_N = 1\,\text{MeV}$ and active-sterile mixing $|V_{eN}|^2 = 0.1$ for ^{76}Ge (left) and ^{136}Xe (right). The shape-factor deviation is non-zero for $\epsilon > m_N$ because of the $1 - |V_{eN}|^2$ suppression of the differential decay rate to light neutrinos in eq. (5.1) and the different normalizations of $S_N(\epsilon)$ and $S_0(\epsilon)$.

for a sterile neutrino with mass $m_N = 1\,\text{MeV}$ and a mixing angle $|V_{eN}|^2 = 0.1$ in figure 8. This value of mixing angle roughly corresponds to limits set by existing $2\nu\beta\beta$ analyses [23, 24], although we stress that stronger limits are presently set by single β-decay spectrum analyses [78, 79]. The spectrum distortion from a sterile neutrino with this mass and mixing is of similar size as the chiral corrections identified in this work. The deviations from the two sources (sterile neutrino and chiral) pull the peak of the spectrum in opposite directions and, for certain parameter setting, could result in mutual cancellation. To be able to resolve sterile neutrino effects in the $2\nu\beta\beta$ spectrum or to set more stringent limits, the chiral corrections must be included in the analysis.

5.2 Non-standard charged-current interactions

Another possible form of BSM physics arises from non-standard charged-current interactions. Several options are possible [80, 81], but we focus here on tensor interactions of left-handed neutrinos and axial and vector couplings of massless right-handed neutrinos. In the conventions of ref. [81], these interactions are captured by the Lagrangian

$$\mathcal{L} = -\frac{4G_F}{\sqrt{2}} V_{ud} \Big\{ \epsilon_T \bar{e}_R \sigma^{\mu\nu} \nu_L \, \bar{u}_R \sigma_{\mu\nu} d_L + \tilde{\epsilon}_R \bar{e}_R \gamma^\mu \nu_R \, \bar{u}_R \gamma_\mu d_R + \tilde{\epsilon}_L \bar{e}_R \gamma^\mu \nu_R \, \bar{u}_L \gamma_\mu d_L \Big\}. \tag{5.6}$$

The couplings $\tilde{\epsilon}_R$ and $\tilde{\epsilon}_L$ are related to ϵ_{RR} and ϵ_{LR} introduced in ref. [17] by $\epsilon_{LR} = -\tilde{\epsilon}_L$, $\epsilon_{RR} = -\tilde{\epsilon}_R$. The operators in eq. (5.6) can be mapped onto gauge invariant operators in the SM Effective Field Theory (SMEFT) [82] or sterile neutrino extended SMEFT (νSMEFT) [83]. In particular, ϵ_T and $\tilde{\epsilon}_R$ correspond, respectively, to semileptonic four-fermion operators in SMEFT and νSMEFT, while $\tilde{\epsilon}_L$ emerges from a coupling of the W boson to right-handed neutrinos and electrons. These interactions can be constrained in low-energy β decays [81, 84–86] and $0\nu\beta\beta$ decays [87]. ϵ_T and $\tilde{\epsilon}_R$ can also be constrained by neutral and charged-current Drell-Yan at the LHC [81, 88], while $\tilde{\epsilon}_L$ can be indirectly constrained by its contribution to lepton dipole moments [89]. Considering only low-energy observables, the global analysis of ref. [85] yields, at the 90% CL

$$-1.2 \cdot 10^{-3} < \epsilon_T < 1.1 \cdot 10^{-3}, \qquad |\tilde{\epsilon}_L + \tilde{\epsilon}_R| < 0.09, \qquad |\tilde{\epsilon}_L - \tilde{\epsilon}_R| < 0.08. \tag{5.7}$$

JHEP06(2025)082

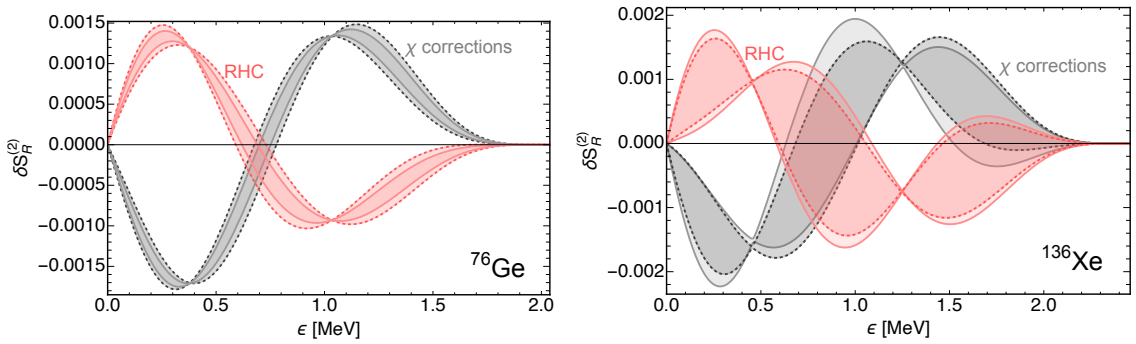

Figure 9. Shape-factor deviations δS induced by the BSM right-handed vector current specified in eq. (5.6) for both Germanium (left) and Xenon (right). Here, we take $|\tilde{\epsilon}_L - \tilde{\epsilon}_R| = 0.1$.

The corrections to the $2\nu\beta\beta$ matrix element is

$$C_{2\nu}^{\rm BSM} = \frac{8g_A^4}{3}\left\{(\tilde{\epsilon}_R - \tilde{\epsilon}_L)^2\left[(M_{GT}^K)^2 + (M_{GT}^L)^2 + M_{GT}^K M_{GT}^L \frac{m_e^2}{E_{e1}E_{e2}}\right]\right.$$
$$\left. + \epsilon_T \frac{g_T}{g_A}\left[(M_{GT}^K)^2 + (M_{GT}^L)^2 + M_{GT}^K M_{GT}^L\right] \frac{m_e(E_{e1}+E_{e2})}{E_{e1}E_{e2}}\right\} \tag{5.8}$$

$$\simeq 8g_A^4 \left(M_{GT}^{(-1)}\right)^2 \left((\tilde{\epsilon}_R - \tilde{\epsilon}_L)^2\left(\frac{2}{3} + \frac{1}{3}\frac{m_e^2}{E_{e1}E_{e2}}\right) + \epsilon_T \frac{g_T}{g_A}\frac{m_e(E_{e1}+E_{e2})}{E_{e1}E_{e2}}\right), \tag{5.9}$$

where we neglected higher-order terms in the $\epsilon_{K,L}$ expansion. Here the isovector tensor charge is [90, 91]

$$g_T = 0.989(34)\,. \tag{5.10}$$

Figure 9 shows the effect of adding a coupling of the nucleon to a leptonic right-handed charged-current (RHC) on the $2\nu\beta\beta$ decay of ^{76}Ge (left) and ^{136}Xe (right). We set $|\tilde{\epsilon}_L - \tilde{\epsilon}_R| = 0.1$, which is close to the bound in eq. (5.7). In red we show the distortion of the spectral shape induced by $|\tilde{\epsilon}_L - \tilde{\epsilon}_R|$, compared to the corrections from WM and the pion-exchange two-neutrino potential, showed in gray. The bands denote the impact of the nuclear uncertainties, dominated by the uncertainty on ξ_{31}. Figure 9 shows that a measurement of the spectrum with 0.1% accuracy could provide a competitive constraint on RHC, and, due to the different shape, the effect cannot be washed out by the nuclear uncertainty on ξ_{31}. The RHC contribution would be of the same size as the chiral corrections, which need to be included to obtain the correct bounds.

Figure 10 shows the effect of a tensor coupling, set to $\epsilon_T = -0.0014$. Also in this case, the effect cannot be mimicked by shifting the value of ξ_{31}, so that a $2\nu\beta\beta$ bound on tensor interactions would not suffer from nuclear theory uncertainties. On the other hand, the tensor distortion has a shape that is very similar to the WM. In particular, a tensor coupling of $\epsilon_T = -0.0014$ would roughly double the shift due to WM, while $\epsilon_T = +0.0014$ would cancel it. Searches for tensor couplings in the $2\nu\beta\beta$ spectrum can thus be competitive with eq. (5.7), and with future searches the β decay spectra of the neutron, ^{6}He and ^{19}Ne [92], but they require the inclusion of chiral corrections, in addition to precise experiments.

JHEP06(2025)082

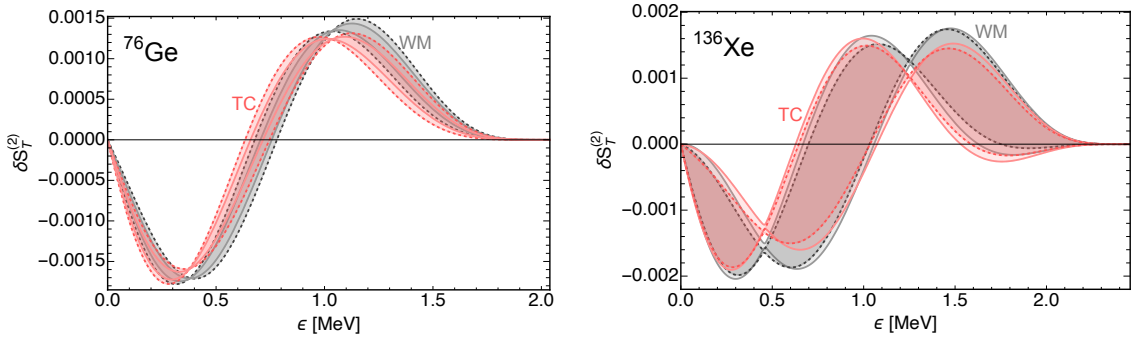

Figure 10. Shape-factor deviations δS induced by the BSM tensor current (TC) with $\epsilon_T = -0.0014$ in comparison with the deviations caused by the weak magnetism (WM) correction term.

6 Conclusion

Next-generation $0\nu\beta\beta$ and dark-matter direct detection experiments will measure a record number of $2\nu\beta\beta$ events, resulting in high precision determination of the electron spectrum. Although often seen as a background, the $2\nu\beta\beta$ electron spectrum is interesting in its own right. In this work, we investigated the electron spectrum in the framework of chiral effective field theory. Our main results can be summarized as follows:

- We computed the leading corrections that appear at $\mathcal{O}(\mathcal{Q}/\Lambda_\chi)$, where $\mathcal{Q}$ is the scale associated to the Q-value of the decay and $\Lambda_\chi \sim$ GeV is the breakdown scale of chiral EFT. The leading corrections can be divided into three contributions. The first arises from the multipole expansion of the weak currents, which receives a first contribution from weak magnetism. The second category consists of double-weak pion-exchange diagrams. The third category are short-range double-weak neutron-neutron-proton-proton-electron-electron-neutrino-neutrino interactions.

- Computing the effect on the (differential) decay rate requires in principle complicated nuclear many-body calculations. This task is somewhat simplified by using the lepton energy expansion of ref. [11]. The corrections from weak magnetism then do not require new NMEs, while the pionic and short-distance effects do require NMEs but these are connected to the same NMEs necessary to describe $0\nu\beta\beta$. This is interesting as it implies that $0\nu\beta\beta$ NMEs can, in principle, be isolated in $2\nu\beta\beta$ measurements. Moreover, two currently unknown contact couplings are required for a full analysis and these may be obtained in the future by Lattice QCD calculations [54, 55].

- As a side result, we have performed a check of the convergence of the lepton energy expansion of ref. [11] in case of the nuclear Shell Model using unexpanded calculations available in the literature. We conclude that the lepton energy expansion converges quickly and is a very useful tool.

- The chiral corrections increase the total decay rates of ^{76}Ge and ^{136}Xe by, respectively, 3% and 10%, but these effects are swamped by the theoretical uncertainty of the total rate computation. We therefore focused on the normalized differential decay spectrum

JHEP06(2025)082

(the shape factor). Weak magnetism corrections are under good theoretical control and they shift the shape factor by a few per-mille over the entire spectrum. The corrections change the peak of the spectrum and can be isolated from nuclear structure corrections arising from subleading terms in the lepton energy expansion. This is in particular true around the nodes, special points in the spectrum where nuclear structure corrections vanish and where ideally the perturbation is maximal.

- The pionic corrections are small for ^{76}Ge and at the few per-mille level for ^{136}Xe, although they might become larger depending on the unknown contributions of the short-distance low-energy constants. They will be harder to identify because their effects are convoluted with nuclear structure corrections to the spectrum. In particular, the largest pionic corrections are proportional to ξ_{31}, a ratio of NMEs, that is poorly known. We have discussed how uncertainties in the NME ratios propagate to uncertainties in the shape factors and how this affects extracting the pionic contributions from data. With the present theoretical control of ξ_{31}, it is difficult to identify the pionic terms from measurements. That being said, a simultaneous fit of the ξ ratios and the pionic corrections might be feasible in the future and we encourage the experimental collaborations to pursue such a fit.

- Precision $2\nu\beta\beta$ spectra measurements have been used to search for BSM physics. We demonstrated that the chiral corrections identified in this work should be included in order to avoid misidentifying BSM physics. In particular, weak magnetism closely resembles an exotic tensor interaction associated to BSM physics at an energy scale around 10 TeV. In addition, per-mille measurements of the electron spectrum could set the most stringent limits on leptonic right-handed charged currents.

- Throughout our analysis of the $2\nu\beta\beta$ spectrum's sensitivity to chiral correction and BSM physics, in contrast with most of the existing literature on the subject, we have taken a rather conservative / realistic approach and have systematically propagated the uncertainty due to nuclear matrix elements, such as the ratio ξ_{31}.

- These corrections do not affect the start or end points of the spectra, but they do impact most of the spectrum away from the nodes. Performing a (nearly) full energy spectrum measurement with a future large detector like XLZD could yield sufficient statistics to measure these corrections.

This first study of $2\nu\beta\beta$ decay using EFT methods has revealed that chiral corrections to the spectra are at the sub-percent level, while corrections to the decay rate can be at the 10% level. In both cases, a full assessment of the impact requires better control of nuclear structure effects. These observations open up several future lines of investigation. While we focused on the energy spectrum, there might be interesting chiral corrections to the angular decay spectrum that can potentially be measured [93]. In addition, the size of chiral corrections to the spectra suggests that control over electromagnetic radiative corrections will ultimately be required to identify the chiral effects. EFT methods have been shown to be beneficial in analyzing radiative corrections to nuclear weak processes [67–69, 94] and can be generalized to study radiative corrections to double weak processes such as $2\nu\beta\beta$.

JHEP06(2025)082

On the other hand, the study of chiral corrections to the decay rate, in conjunction with first-principles nuclear structure calculations, can lead in the future to precise predictions for the $2\nu\beta\beta$ decay rates across a number of isotopes, thus increasing our confidence on the whole methodology used to study the corresponding neutrino-less decays.

Acknowledgments

We thank Maxime Pierre, Auke-Pieter Colijn, Javier Menéndez and Ralph Massarczyk for useful discussions and encouragement. Financial support by the Dutch Research Council (NWO) in the form of a VIDI grant, the U.S. DOE (Grant No. DE-FG02-00ER41132), and Los Alamos National Laboratory's Laboratory Directed Research and Development program under projects 20250164ER and 20230047DR is gratefully acknowledged. We also acknowledge support from the Dutch Research Council (NWO), under project number VI.Veni.222.318 and from Charles University through project PRIMUS/24/SCI/013. Los Alamos National Laboratory is operated by Triad National Security, LLC, for the National Nuclear Security Administration of U.S. Department of Energy (Contract No. 89233218CNA000001). We acknowledge support from the DOE Topical Collaboration "Nuclear Theory for New Physics," award No. DE-SC0023663. This material is based, in part, on work supported by the U.S. Department of Energy, Office of Science, Office of Workforce Development for Teachers and Scientists, Office of Science Graduate Student Research (SCGSR) program, under contract number DE-SC0014664.

Data Availability Statement. This article has no associated data or the data will not be deposited.

Code Availability Statement. This article has no associated code or the code will not be deposited.

Open Access. This article is distributed under the terms of the Creative Commons Attribution License (CC-BY4.0), which permits any use, distribution and reproduction in any medium, provided the original author(s) and source are credited.

References

[1] A. Barabash, *Double Beta Decay Experiments: Recent Achievements and Future Prospects*, *Universe* **9** (2023) 290.

[2] XENON collaboration, *Observation of two-neutrino double electron capture in ^{124}Xe with XENON1T*, *Nature* **568** (2019) 532 [arXiv:1904.11002] [INSPIRE].

[3] GERDA collaboration, *Final Results of GERDA on the Two-Neutrino Double-β Decay Half-Life of Ge76*, *Phys. Rev. Lett.* **131** (2023) 142501 [arXiv:2308.09795] [INSPIRE].

[4] M. Agostini et al., *Toward the discovery of matter creation with neutrinoless $\beta\beta$ decay*, *Rev. Mod. Phys.* **95** (2023) 025002 [arXiv:2202.01787] [INSPIRE].

[5] C. Adams et al., *Neutrinoless Double Beta Decay*, arXiv:2212.11099 [INSPIRE].

[6] KamLAND-Zen collaboration, *Search for Majorana Neutrinos with the Complete KamLAND-Zen Dataset*, arXiv:2406.11438 [INSPIRE].

JHEP06(2025)082

[7] CUPID collaboration, *CUPID pre-CDR*, arXiv:1907.09376 [INSPIRE].

[8] NEXO collaboration, *nEXO Pre-Conceptual Design Report*, arXiv:1805.11142 [INSPIRE].

[9] LEGEND collaboration, *The Large Enriched Germanium Experiment for Neutrinoless $\beta\beta$ Decay: LEGEND-1000 Preconceptual Design Report*, arXiv:2107.11462 [INSPIRE].

[10] XENON collaboration, *Double-Weak Decays of ^{124}Xe and ^{136}Xe in the XENON1T and XENONnT Experiments*, Phys. Rev. C **106** (2022) 024328 [arXiv:2205.04158] [INSPIRE].

[11] F. Šimkovic, R. Dvornický, D. Stefánik and A. Faessler, *Improved description of the $2\nu\beta\beta$ -decay and a possibility to determine the effective axial-vector coupling constant*, Phys. Rev. C **97** (2018) 034315 [arXiv:1804.04227] [INSPIRE].

[12] KAMLAND-ZEN collaboration, *Precision measurement of the ^{136}Xe two-neutrino $\beta\beta$ spectrum in KamLAND-Zen and its impact on the quenching of nuclear matrix elements*, Phys. Rev. Lett. **122** (2019) 192501 [arXiv:1901.03871] [INSPIRE].

[13] M. Doi, T. Kotani and E. Takasugi, *The Neutrinoless Double Beta Decay With Majoron Emission*, Phys. Rev. D **37** (1988) 2575 [INSPIRE].

[14] C.P. Burgess and J.M. Cline, *Majorons without Majorana masses and neutrinoless double beta decay*, Phys. Lett. B **298** (1993) 141 [hep-ph/9209299] [INSPIRE].

[15] C.P. Burgess and J.M. Cline, *A New class of Majoron emitting double beta decays*, Phys. Rev. D **49** (1994) 5925 [hep-ph/9307316] [INSPIRE].

[16] K. Blum, Y. Nir and M. Shavit, *Neutrinoless double-beta decay with massive scalar emission*, Phys. Lett. B **785** (2018) 354 [arXiv:1802.08019] [INSPIRE].

[17] F.F. Deppisch, L. Graf and F. Šimkovic, *Searching for New Physics in Two-Neutrino Double Beta Decay*, Phys. Rev. Lett. **125** (2020) 171801 [arXiv:2003.11836] [INSPIRE].

[18] F.F. Deppisch, L. Graf, W. Rodejohann and X.-J. Xu, *Neutrino Self-Interactions and Double Beta Decay*, Phys. Rev. D **102** (2020) 051701 [arXiv:2004.11919] [INSPIRE].

[19] P.D. Bolton, F.F. Deppisch, L. Gráf and F. Šimkovic, *Two-Neutrino Double Beta Decay with Sterile Neutrinos*, Phys. Rev. D **103** (2021) 055019 [arXiv:2011.13387] [INSPIRE].

[20] M. Agostini, E. Bossio, A. Ibarra and X. Marcano, *Search for Light Exotic Fermions in Double-Beta Decays*, Phys. Lett. B **815** (2021) 136127 [arXiv:2012.09281] [INSPIRE].

[21] O. Nitescu, S. Ghinescu and S. Stoica, *Lorentz violation effects in $2\nu\beta\beta$ decay*, J. Phys. G **47** (2020) 055112 [arXiv:2001.04859] [INSPIRE].

[22] M. Agostini et al., *Results on $\beta\beta$ decay with emission of two neutrinos or Majorons in^{76} Ge from GERDA Phase I*, Eur. Phys. J. C **75** (2015) 416 [arXiv:1501.02345] [INSPIRE].

[23] CUPID collaboration, *Searching for beyond the Standard Model physics using the improved description of ^{100}Mo $2\nu\beta\beta$ decay spectral shape with CUPID-Mo*, Eur. Phys. J. C **84** (2024) 925 [arXiv:2405.10766] [INSPIRE].

[24] GERDA collaboration, *Search for exotic physics in double-β decays with GERDA Phase II*, JCAP **12** (2022) 012 [arXiv:2209.01671] [INSPIRE].

[25] S.A. Kharusi et al., *Search for Majoron-emitting modes of ^{136}Xe double beta decay with the complete EXO-200 dataset*, Phys. Rev. D **104** (2021) 112002 [arXiv:2109.01327] [INSPIRE].

[26] CUPID-0 collaboration, *Search for Majoron-like particles with CUPID-0*, Phys. Rev. D **107** (2023) 032006 [arXiv:2209.09490] [INSPIRE].

JHEP06(2025)082

[27] J.S. Diaz, *Limits on Lorentz and CPT violation from double beta decay*, *Phys. Rev. D* **89** (2014) 036002 [arXiv:1311.0930] [INSPIRE].

[28] J.S. Díaz, A. Kostelecký and R. Lehnert, *Relativity violations and beta decay*, *Phys. Rev. D* **88** (2013) 071902 [arXiv:1305.4636] [INSPIRE].

[29] M. Doi, T. Kotani and E. Takasugi, *Double Beta Decay and Majorana Neutrino*, *Prog. Theor. Phys. Suppl.* **83** (1985) 1.

[30] J. Kotila and F. Iachello, *Phase space factors for double-β decay*, *Phys. Rev. C* **85** (2012) 034316 [arXiv:1209.5722] [INSPIRE].

[31] O. Niţescu and F. Šimkovic, *Radiative and exchange corrections for two-neutrino double-β decay*, *Phys. Rev. C* **111** (2025) 035501 [arXiv:2411.05405] [INSPIRE].

[32] S. Weinberg, *Effective chiral Lagrangians for nucleon-pion interactions and nuclear forces*, *Nucl. Phys. B* **363** (1991) 3 [INSPIRE].

[33] V. Cirigliano et al., *New Leading Contribution to Neutrinoless Double-β Decay*, *Phys. Rev. Lett.* **120** (2018) 202001 [arXiv:1802.10097] [INSPIRE].

[34] R. Wirth, J.M. Yao and H. Hergert, *Ab Initio Calculation of the Contact Operator Contribution in the Standard Mechanism for Neutrinoless Double Beta Decay*, *Phys. Rev. Lett.* **127** (2021) 242502 [arXiv:2105.05415] [INSPIRE].

[35] A. Belley et al., *Ab initio Uncertainty Quantification of Neutrinoless Double-Beta Decay in Ge76*, *Phys. Rev. Lett.* **132** (2024) 182502 [arXiv:2308.15634] [INSPIRE].

[36] C. Barbero, F. Krmpotic, A. Mariano and D. Tadic, *Weak magnetism in two neutrino double beta decay*, *Phys. Lett. B* **445** (1999) 249 [nucl-th/9810072] [INSPIRE].

[37] K. Amos, A. Faessler and V. Rodin, *Charge-exchange reaction cross sections and the Gamow-Teller strength for double beta decay*, *Phys. Rev. C* **76** (2007) 014604 [nucl-th/0702016] [INSPIRE].

[38] E. Santopinto, H. García-Tecocoatzi, R.I. Magaña Vsevolodovna and J. Ferretti, *Heavy-ion double-charge-exchange and its relation to neutrinoless double-β decay*, *Phys. Rev. C* **98** (2018) 061601 [arXiv:1806.03069] [INSPIRE].

[39] NUMEN collaboration, *Shedding light on nuclear aspects of neutrinoless double beta decay by heavy-ion double charge exchange reactions*, *Prog. Part. Nucl. Phys.* **128** (2023) 103999 [INSPIRE].

[40] N. Shimizu, J. Menéndez and K. Yako, *Double Gamow-Teller Transitions and its Relation to Neutrinoless $\beta\beta$ Decay*, *Phys. Rev. Lett.* **120** (2018) 142502 [arXiv:1709.01088] [INSPIRE].

[41] J.M. Yao et al., *Ab initio studies of the double-Gamow-Teller transition and its correlation with neutrinoless double-β decay*, *Phys. Rev. C* **106** (2022) 014315 [arXiv:2204.12971] [INSPIRE].

[42] L. Jokiniemi and J. Menéndez, *Correlations between neutrinoless double-β, double Gamow-Teller, and double-magnetic decays in the proton-neutron quasiparticle random-phase approximation framework*, *Phys. Rev. C* **107** (2023) 044316 [arXiv:2302.05399] [INSPIRE].

[43] A. Belley et al., *Correlation of neutrinoless double-beta decay nuclear matrix elements with nucleon-nucleon phase shifts*, arXiv:2408.02169 [INSPIRE].

[44] B. Romeo, J. Menéndez and C. Peña Garay, *$\gamma\gamma$ decay as a probe of neutrinoless $\beta\beta$ decay nuclear matrix elements*, *Phys. Lett. B* **827** (2022) 136965 [arXiv:2102.11101] [INSPIRE].

[45] B. Romeo, D. Stramaccioni, J. Menéndez and J.J. Valiente-Dobón, *A pathway to unveiling neutrinoless $\beta\beta$ decay nuclear matrix elements via $\gamma\gamma$ decay*, *Phys. Lett. B* **860** (2025) 139186 [arXiv:2411.03539] [INSPIRE].

JHEP06(2025)082

[46] W.C. Haxton and G.J. Stephenson, *Double beta Decay*, *Prog. Part. Nucl. Phys.* **12** (1984) 409 [INSPIRE].

[47] T.W. Donnelly and J.D. Walecka, *Electron Scattering and Nuclear Structure*, *Ann. Rev. Nucl. Part. Sci.* **25** (1975) 329 [INSPIRE].

[48] J.D. Walecka, *Theoretical nuclear and subnuclear physics*, *Oxford Stud. Nucl. Phys.* **16** (1995) 1 [INSPIRE].

[49] V. Bernard, N. Kaiser and U.-G. Meissner, *Chiral dynamics in nucleons and nuclei*, *Int. J. Mod. Phys. E* **4** (1995) 193 [hep-ph/9501384] [INSPIRE].

[50] D.B. Kaplan, M.J. Savage and M.B. Wise, *Nucleon-nucleon scattering from effective field theory*, *Nucl. Phys. B* **478** (1996) 629 [nucl-th/9605002] [INSPIRE].

[51] B. Borasoy and H.W. Griesshammer, *The S wave pion deuteron scattering length in effective field theory*, nucl-th/0105048 [INSPIRE].

[52] V. Cirigliano, M. Dawid, W. Dekens and S. Reddy, *A New Class of Three Nucleon Forces and their Implications*, arXiv:2411.00097 [INSPIRE].

[53] V. Cirigliano et al., *Renormalized approach to neutrinoless double-β decay*, *Phys. Rev. C* **100** (2019) 055504 [arXiv:1907.11254] [INSPIRE].

[54] P.E. Shanahan et al., *Isotensor Axial Polarizability and Lattice QCD Input for Nuclear Double-β Decay Phenomenology*, *Phys. Rev. Lett.* **119** (2017) 062003 [arXiv:1701.03456] [INSPIRE].

[55] B.C. Tiburzi et al., *Double-β Decay Matrix Elements from Lattice Quantum Chromodynamics*, *Phys. Rev. D* **96** (2017) 054505 [arXiv:1702.02929] [INSPIRE].

[56] V. Cirigliano et al., *Neutrinoless double beta decay in chiral effective field theory: lepton number violation at dimension seven*, *JHEP* **12** (2017) 082 [arXiv:1708.09390] [INSPIRE].

[57] J. Barea, J. Kotila and F. Iachello, *$0\nu\beta\beta$ and $2\nu\beta\beta$ nuclear matrix elements in the interacting boson model with isospin restoration*, *Phys. Rev. C* **91** (2015) 034304 [arXiv:1506.08530] [INSPIRE].

[58] J. Hyvärinen and J. Suhonen, *Nuclear matrix elements for $0\nu\beta\beta$ decays with light or heavy Majorana-neutrino exchange*, *Phys. Rev. C* **91** (2015) 024613 [INSPIRE].

[59] J. Menéndez, *Neutrinoless $\beta\beta$ decay mediated by the exchange of light and heavy neutrinos: The role of nuclear structure correlations*, *J. Phys. G* **45** (2018) 014003 [arXiv:1804.02105] [INSPIRE].

[60] M. Blennow, E. Fernandez-Martinez, J. Lopez-Pavon and J. Menendez, *Neutrinoless double beta decay in seesaw models*, *JHEP* **07** (2010) 096 [arXiv:1005.3240] [INSPIRE].

[61] A. Faessler, M. González, S. Kovalenko and F. Šimkovic, *Arbitrary mass Majorana neutrinos in neutrinoless double beta decay*, *Phys. Rev. D* **90** (2014) 096010 [arXiv:1408.6077] [INSPIRE].

[62] J. Barea, J. Kotila and F. Iachello, *Limits on sterile neutrino contributions to neutrinoless double beta decay*, *Phys. Rev. D* **92** (2015) 093001 [arXiv:1509.01925] [INSPIRE].

[63] W. Dekens et al., *Neutrinoless double-β decay in the neutrino-extended standard model*, *Phys. Rev. C* **108** (2023) 045501 [arXiv:2303.04168] [INSPIRE].

[64] W. Dekens et al., *Neutrinoless double beta decay rates in the presence of light sterile neutrinos*, *JHEP* **09** (2024) 201 [arXiv:2402.07993] [INSPIRE].

[65] L. Hayen et al., *High precision analytical description of the allowed β spectrum shape*, *Rev. Mod. Phys.* **90** (2018) 015008 [arXiv:1709.07530] [INSPIRE].

JHEP06(2025)082

[66] D.H. Wilkinson, *Methodology for superallowed Fermi beta decay. 2. Reduction of data*, *Nucl. Instrum. Meth. A* **335** (1993) 182 [INSPIRE].

[67] R.J. Hill and R. Plestid, *Field Theory of the Fermi Function*, *Phys. Rev. Lett.* **133** (2024) 021803 [arXiv:2309.07343] [INSPIRE].

[68] R.J. Hill and R. Plestid, *All orders factorization and the Coulomb problem*, *Phys. Rev. D* **109** (2024) 056006 [arXiv:2309.15929] [INSPIRE].

[69] V. Cirigliano et al., *Ab initio electroweak corrections to superallowed β decays and their impact on Vud*, *Phys. Rev. C* **110** (2024) 055502 [arXiv:2405.18464] [INSPIRE].

[70] F. Salvat and J. M. Fernández-Varea, *RADIAL: A Fortran subroutine package for the solution of the radial Schrödinger and Dirac wave equations*, *Comput. Phys. Commun.* **240** (2019) 165.

[71] L. Jokiniemi, B. Romeo, P. Soriano and J. Menéndez, *Neutrinoless $\beta\beta$-decay nuclear matrix elements from two-neutrino $\beta\beta$-decay data*, *Phys. Rev. C* **107** (2023) 044305 [arXiv:2207.05108] [INSPIRE].

[72] J. Menendez, D. Gazit and A. Schwenk, *Chiral two-body currents in nuclei: Gamow-Teller transitions and neutrinoless double-beta decay*, *Phys. Rev. Lett.* **107** (2011) 062501 [arXiv:1103.3622] [INSPIRE].

[73] E. Caurier, F. Nowacki and A. Poves, *Shell Model description of the beta beta decay of 136Xe*, *Phys. Lett. B* **711** (2012) 62 [arXiv:1112.5039] [INSPIRE].

[74] E.A. Coello Pérez, J. Menéndez and A. Schwenk, *Two-neutrino double electron capture on ^{124}Xe based on an effective theory and the nuclear shell model*, *Phys. Lett. B* **797** (2019) 134885 [arXiv:1809.04443] [INSPIRE].

[75] EXO-200 collaboration, *Improved measurement of the $2\nu\beta\beta$ half-life of ^{136}Xe with the EXO-200 detector*, *Phys. Rev. C* **89** (2014) 015502 [arXiv:1306.6106] [INSPIRE].

[76] S. Novario et al., *Coupled-Cluster Calculations of Neutrinoless Double-β Decay in ^{48}Ca*, *Phys. Rev. Lett.* **126** (2021) 182502 [arXiv:2008.09696] [INSPIRE].

[77] V. Cirigliano et al., *A neutrinoless double beta decay master formula from effective field theory*, *JHEP* **12** (2018) 097 [arXiv:1806.02780] [INSPIRE].

[78] J. Deutsch, M. Lebrun and R. Prieels, *Searches for admixture of massive neutrinos into the electron flavour*, *Nucl. Phys. A* **518** (1990) 149.

[79] P.D. Bolton, F.F. Deppisch and P.S. Bhupal Dev, *Neutrinoless double beta decay versus other probes of heavy sterile neutrinos*, *JHEP* **03** (2020) 170 [arXiv:1912.03058] [INSPIRE].

[80] T.D. Lee and C.-N. Yang, *Question of Parity Conservation in Weak Interactions*, *Phys. Rev.* **104** (1956) 254 [INSPIRE].

[81] V. Cirigliano, M. Gonzalez-Alonso and M.L. Graesser, *Non-standard Charged Current Interactions: beta decays versus the LHC*, *JHEP* **02** (2013) 046 [arXiv:1210.4553] [INSPIRE].

[82] B. Grzadkowski, M. Iskrzynski, M. Misiak and J. Rosiek, *Dimension-Six Terms in the Standard Model Lagrangian*, *JHEP* **10** (2010) 085 [arXiv:1008.4884] [INSPIRE].

[83] F. del Aguila, S. Bar-Shalom, A. Soni and J. Wudka, *Heavy Majorana Neutrinos in the Effective Lagrangian Description: Application to Hadron Colliders*, *Phys. Lett. B* **670** (2009) 399 [arXiv:0806.0876] [INSPIRE].

[84] V. Cirigliano, S. Gardner and B. Holstein, *Beta Decays and Non-Standard Interactions in the LHC Era*, *Prog. Part. Nucl. Phys.* **71** (2013) 93 [arXiv:1303.6953] [INSPIRE].

JHEP06(2025)082

[85] A. Falkowski, M. González-Alonso and O. Naviliat-Cuncic, *Comprehensive analysis of beta decays within and beyond the Standard Model*, *JHEP* **04** (2021) 126 [arXiv:2010.13797] [INSPIRE].

[86] W. Dekens et al., *Sterile neutrinos and neutrinoless double beta decay in effective field theory*, *JHEP* **06** (2020) 097 [arXiv:2002.07182] [INSPIRE].

[87] W. Dekens, J. de Vries and T. Tong, *Sterile neutrinos with non-standard interactions in β- and $0\nu\beta\beta$-decay experiments*, *JHEP* **08** (2021) 128 [arXiv:2104.00140] [INSPIRE].

[88] S. Alioli, W. Dekens, M. Girard and E. Mereghetti, *NLO QCD corrections to SM-EFT dilepton and electroweak Higgs boson production, matched to parton shower in POWHEG*, *JHEP* **08** (2018) 205 [arXiv:1804.07407] [INSPIRE].

[89] V. Cirigliano et al., *Leptonic anomalous magnetic moments in ν SMEFT*, *JHEP* **08** (2021) 103 [arXiv:2105.11462] [INSPIRE].

[90] R. Gupta et al., *Isovector Charges of the Nucleon from 2+1+1-flavor Lattice QCD*, *Phys. Rev. D* **98** (2018) 034503 [arXiv:1806.09006] [INSPIRE].

[91] Flavour Lattice Averaging Group collaboration, *FLAG Review 2021*, *Eur. Phys. J. C* **82** (2022) 869 [arXiv:2111.09849] [INSPIRE].

[92] M. Brodeur et al., *Nuclear β decay as a probe for physics beyond the Standard Model*, arXiv:2301.03975 [INSPIRE].

[93] SuperNEMO collaboration, *Probing New Physics Models of Neutrinoless Double Beta Decay with SuperNEMO*, *Eur. Phys. J. C* **70** (2010) 927 [arXiv:1005.1241] [INSPIRE].

[94] V. Cirigliano et al., *Radiative Corrections to Superallowed β Decays in Effective Field Theory*, *Phys. Rev. Lett.* **133** (2024) 211801 [arXiv:2405.18469] [INSPIRE].

JHEP06(2025)082